The Cause and Morphology of Fracture in Acetal Quick Disconnect Couplings used in a Residential Water Filter Application

A DISSERTATION
SUBMITTED TO THE FACULTY OF THE GRADUATE SCHOOL
OF THE UNIVERSITY OF MINNESOTA
BY

Jeremy Henry Nichols

IN PARTIAL FULFILLMENT OF THE REQUIREMENTS
FOR THE DEGREE OF
Master of Materials Science and Engineering

Advisor: William Gerberich

June 2012

Acknowledgements:

I would like to acknowledge the contributions of many others in helping to make this thesis possible. First, I would like to thank my advisor, Bill Gerberich, who has been instrumental in helping me to refine and better develop my experimental interpretations. I would like to thank Kelly Hoverston for legal research and assistance with the liability section, much of which is taken from a series of letters to claimants and plaintiffs we have written together over the last 3 years. Thanks also to Jeff Domler, Peter deCler, and Mary Wallraff from Colder Products for their assistance with the ongoing issues related to the product returns this work is focused on. Last but not least, thanks to Dieter Scholtz, Bill Mook and Megan Cordill, who helped prepare and perform SEM on some of the samples used.

Dedication:

This work is dedicated to my wife, SarahJane, who encouraged, inspired, and motivated me to undertake and complete it.

Introduction:

The present work is aimed at achieving a fuller understanding of the cause of one mode of failure of a component used in residential water filtration. In 1993, a company called Ametek introduced a residential water filtration system for use with refrigerators with in-the-door ice and water dispensers. These filters are meant to remove common impurities such as chlorine and minerals from tap water. Each filter has a useful life of between six to twelve months after which it must be replaced.

In order to make the task of filter replacement faster and easier Ametek and later other companies engaged in the same line of business elected to provide quick disconnect couplings with the filters to allow easier changes. Generally, this was performed by plumbing the filter behind the refrigerator, under a sink, or in some other inconspicuous yet convenient space.

A quick disconnect coupling (or, simply, a coupling) is a type of fluid connector that allows equipment or fluid lines to be connected and disconnected quickly and without the use of tools. Couplings are generally used in fluid or air handling systems where service requirements necessitate breaking and making connections in the system easily. For instance, a workshop may have a variety of tools that are air driven which are needed at various times. Rather than installing a hard plumbing connection each time a

tool must be changed, one half of a quick disconnect coupling may be installed on the air supply outlet and a mating half may be fitted to each tool. When a need to transition from using one tool to another arises, the quick disconnect coupling on the tool in use can be easily disconnected, and the mating component on the newly required tool can be clicked into place in a matter of moments.

The coupling chosen by Ametek, which later gained acceptance from other manufacturers, was produced by the author's present employer, Colder Products Company. The component selected was Colder's APC (all-plastic coupling.) This product was unique in the market at that time, owing to its simple two-piece, single material, all injection molded plastic design. The parts were originally designed for general industrial and chemical use in applications such as air and water lines, compression therapy devices, cooling circuits and heat exchange systems, and laboratory equipment, among others.

In 1995, after less than two years in the field, Ametek began receiving claims from insurance companies. Filter systems installed in the field were failing, releasing water and causing damage which the insurance companies were paying to repair. After paying contractors to repair any damage, the insurers were pursuing Ametek for the dollar value of the losses. In time, they began to pursue Colder as well because Colder's couplings were fracturing in some of these losses.

Colder has been defending against such claims since 1995. Often, claims are substantiated by reports prepared by third party analysts who have evaluated parts involved in such losses. However, their analyses have generally lacked scientific rigor, making claims based more upon assertion than upon documented testing, calculation, and analysis. The purpose of this thesis is to more rigorously explore the fractures observed in such parts and scientifically determine the most likely cause of one of the failure modes seen in the field, and to develop a master comparison to enable fracture surfaces of broken parts to reference images to determine the mechanism of crack propagation involved in a given break.

Thesis Organization:

The present work begins with an introduction to the history of the project and the nature of the parts being considered in order to lay a foundational understanding for the material to follow. Next, an analysis of the various types and degrees of loading that may be encountered in the field is presented to investigate the types of stress that must be considered, followed by the legal and economic ramifications of part breakage in the field.

Next, the chemistry and material properties of the acetal material used to fabricate the couplings will be considered in terms of its advantages, disadvantages, and suitability.

The thesis will conclude with an analysis of several parts that were intentionally exposed to specific, singular load conditions (fatigue loading, creep, and overload) to generate intentional failures. These parts were extensively characterized in order to identify specific features that are characteristic of that failure mode in order to enable accurate determination of the cause of fracture in samples with unknown stress histories, and these features are reviewed in detail. Finally, conclusions will be offered along with recommendations for future study.

Contents

List of Figures

List of Tables

Part History:

In order to provide maximum clarity for the reader in further exploring the present thesis, it is prudent to provide an overview of the APC coupling that will be evaluated in later sections.

Figure 1: Exemplar APC couplings. A coupling consists of a male and female component, which are joined by a locking mechanism. Body (female) components are shown on the top row. Insert (male) components are shown on the bottom row.

The APC product was not designed especially for use in water filtration. Originally it was conceived as a replacement for multi-component couplings that consisted of metal latching mechanisms and plastic wetted components. Examples of different APC couplings are shown in Figure 1. By introducing a new latching technology with integrated cantilever springs in the locking component (called a clip, or thumblatch), significant cost savings were achieved compared to earlier designs.

Several different versions of the APC have been developed which employ different terminations, allowing the couplings to be connected to different mating components. For example, some parts use hose barbs to allow soft plastic tubing to be pushed over the back of the coupling, where it seals in place. Others use pipe threads allowing the coupling component to be screwed into place. Still others have a PTF termination which allows a metal nut to compress and trap soft plastic tubing on a miniature hosebarb.

Many of these configurations are standard products, while other configurations have been made available as custom products. In addition to offering a fixed catalog of parts for sale, Colder Products Company also makes it a practice to offer custom versions of its standard product to customers who have special requirements. For example, a customer may have a need for a coupling with a non-standard termination, perhaps using a different thread design to mate to some part of their own. Colder would then design and produce a variant on the standard product to meet the specific requirements of that customer. This is the process that led to the development of a coupling for the water filtration application.

The specific parts developed for water filtration applications were custom parts. Specifically, in order to be used in residential plumbing applications, the APC would need to be able to mate to standard ¼" OD copper tubing used in residential plumbing. This required Colder to build tooling to match SAE specifications for such connections.

The APC couplings developed for Ametek were then incorporated into a filter assembly containing parts not made by Colder. Figure 2 shows a diagram of the filter assembly as a whole. Again to enhance clarity, it is useful to indicate the name and material of each component, and who produces it. This information is presented in Table 1.

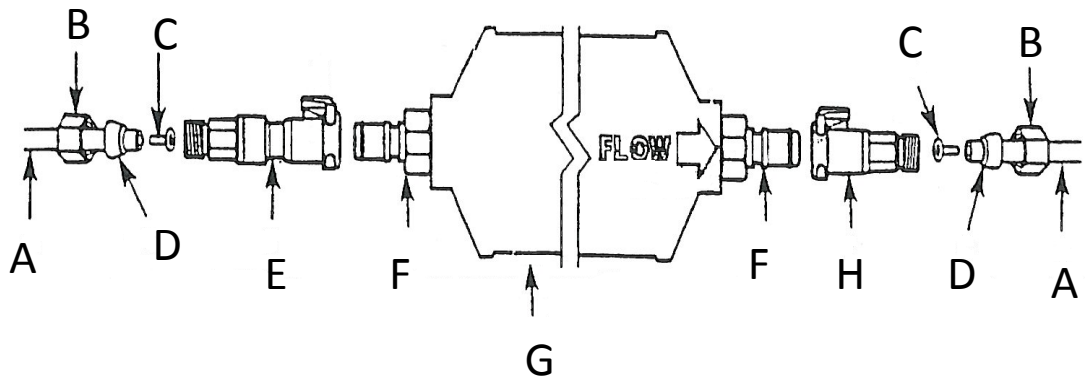

Figure 2: Image taken from GE Appliances instructions for a filter kit; modified to enhance clarity. This graphic illustrates the components included in a water filter assembly. Components E, F and H are produced by Colder, while the rest are supplied by others, while a filter manufacturer assembles the components into a finished product.

Table 1: This table indicates the manufacturer and material of each of the components used in a typical installation.

Letter	Component Name, material	Produced by
A	Water supply line, copper or polyethylene	Other, not included in kits
B	Compression nut, brass	Other, included in kits
C	Reinforcing Insert, Brass (used with polyethylene tubing)	Other, included in kits
D	Ferrule (brass or polyethylene)	Other, included in kits
E	Valved APC series body, acetal	Colder Products Company
F	Non-valved APC series insert	Colder Products Company
G	Filter Cartridge	Ametek, Sta-Rite, *et al*
H	Non-valved APC series body	Colder Products Company

The use of quick disconnect couplings in this application allowed the homeowner to replace their filters much more easily than had the product been hard plumbed into place. An additional benefit was achieved through the use of an automatic shutoff valve in one of the bodies (the one intended to be installed on the water supply side). The shut off valve would automatically stop the flow of water through the coupling upon disconnection through the use of a spring-driven valve. On connection, the insert would push this valve into the open position, but upon disconnection, the valve would automatically move back to the closed position, stopping water flow. This allowed the filter to be replaced in a "hot swap" fashion with no need to manually turn off the flow of water to the refrigerator using a separate valve.

The water filter assembly is often installed by a consumer rather than a professional plumber or other skilled or semi-skilled tradesperson. The installer is provided with the filter, couplings, related hardware, and a set of instructions by the filter manufacturer. An example of the instructions provided are shown in Appendix A.

As with any consumer product, significant variations in installation conditions exist. Some parts are doubtless exposed to more adverse conditions than others. The instructions call for the water filter to be installed behind the refrigerator. Many homeowners, however, seem to deviate from this method, often locating the filter

under a sink, in a wall cavity, or between rafters. Even when the filter is installed in the correct location, it is often not installed within the recommended parameters.

This variation in installation conditions may play a role in causing some couplings to fracture. Several possibilities are easily imagined that would lead to extreme loading of the coupling and the filter. For instance, if the filter were installed as directed behind the refrigerator, the filter will prevent the refrigerator from being restored to its original position, tight against the wall. This results in the appliance jutting forward from the countertop more than may be desired. If a homeowner were to be dissatisfied with this situation, and less than careful about his analysis of the problem, he may through some violence attempt to move to refrigerator back to its original position, applying considerable force to the appliance, and therefore to the filter and tubing assembly behind it.

Additionally, when the refrigerator is moved away from the wall, a short piece of tubing could result in the entire momentum of the moving appliance being arrested by the water supply line, transmitting that kinetic energy into the deformation of tubing, and loading the couplings as well.

Other possible scenarios can also be imagined, including the repetitive furling and unfurling of the tubing under a sink or in a wall cavity as the filter is extracted from its tight space for a change of the cartridge.

These various scenarios, and others not postulated, have yielded claims on roughly 1 part in 50,000 sold by Colder into this market. This ratio is quite small, however, when one accounts for the fact that over 20,000,000 parts have been sold over the past 16 years, the total number is nontrivial. Several different failure modes affecting different portions of the coupling components have been observed, however, the scope of this document will include only one of these.

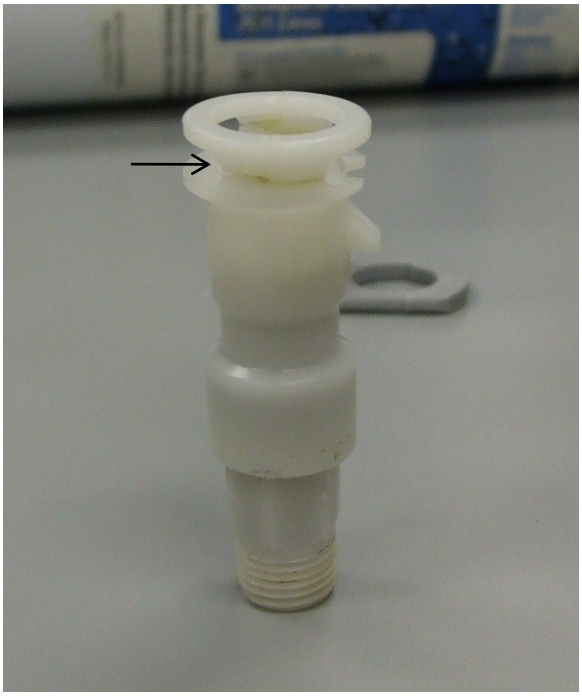

Figure 3: Photograph showing the location of the crack in the mode of interest to this analysis. The crack passes through the "ears" responsible for retaining the latching mechanism. An arrow indicates the crack location in the figure.

The mode of interest in this thesis is the fracture of one of the two the body components at the section which is responsible for retaining the locking clip. This area is referred to as the “ears” of the body, and is the region noted in Figure 3. The ears join the main body of the component to the ring-like face of the part that encloses and secures the locking clip. A break through the ears will release the locking clip from the body and allow a coupling insert to be ejected, breaking the connection. This break can occur on either the valved or non-valved body component; both parts have the same clip component, and the geometry of the plastic retaining the clip is the same in both as well.

The non-valved component fracturing would result in the release of water. The fracture of the valved component may not result in the release of water, however. When properly installed on the water supply line (as opposed to the appliance side of the filter), a break in this location would result only in the disconnection of the body and insert components. A spring activated poppet valve inside the body would be driven against its seat upon disconnection, which would halt the flow of water and prevent damage.

This failure mode is common only to the first type of couplings in the water filter application; therefore this is the type of product that will be the subject of the present analysis.

Load Analysis

A break at the ears implies some form of excessive stress in them, which can arise from several sources:

1.) The fluid pressure in the coupling, which acts to force the coupling apart and is resisted by the thumblatch. This force should total less than 15 pounds with the 80 PSI pressure that is the typical maximum in residential plumbing.

2.) The force of the spring pushing out on the insert in the cases where the fractured part is the valved body. (No spring is present in the non-valved body.) This force is additive with the effect of fluid pressure, and contributes 2.8 pounds.

3.) Water hammer forces from the dissipation of the kinetic energy of water flowing through the filter. This effect is expected to be small because the low flow rate of water through the filter prevents significant kinetic energy from being developed.

The calculation for water hammer requires use of the equation:

$$\Delta P = \frac{I}{20\ D^2}\alpha\sqrt{S * B}$$

Equation 1

(The Lee Company, 2009)

Where:

ΔP = Pressure change (spike) due to kinetic effects of arresting a flowing liquid
I = Flow rate, in GPM
D = Inside diameter of fluid path upstream from the component, in inches
S = Specific gravity of medium (In this case, 1 for water)
B = Bulk modulus of liquid (310,000 PSI) (The Lee Company, 2009)
α = a dimensional constant

Defining the values of the variable parameters is straightforward. For ¼" OD tubing, the largest ID that is commonly available is .19". The filters commonly used with these connectors have a stated flow rate of 0.5 GPM.

$$\Delta P = \frac{0.5}{20\ (.19)^2}\sqrt{1 * 310000}$$

$$\Delta P = \frac{0.5\ gallons/min}{.722 in^2}556$$

$$\Delta P = 385$$

This calculation assumes a rigid system, with no volumetric expansion available to absorb the energy of the moving liquid. The use of plastic tubing, or even the flexing of the filter cartridge itself, along with any tubing elsewhere in the system inside the appliance itself will allow the momentum of the flowing water to be dissipated in other components, reducing the magnitude of this force.

The Water Quality Association prescribes a water hammer test simulation 20 years of service (100,000 pressure spikes) and the filter system passed this testing. This indicates that the water hammer is not likely to be a primary source of failure. However, it may contribute stress to the overall system.

4.) Tensile and bending forces from the filter installation. This is expected to be especially large in instances where the filter position is fixed and semi-rigid copper tubing is used to plumb the supply line because cold working as a result of filter changes can significantly increase the rigidity of the tubing. It is discussed in more detail later in the analysis.

Environment:

The environment the product is exposed to is generally considered to be benign. The ears are never exposed to liquid from the water line because they are out of the flowpath of the part, so environmentally assisted cracking based upon chlorine or other contaminants in the water are not contenders for root cause.

The temperatures encountered in the application are expected to be slightly above room temperatures owing to the installation occurring in a home environment where the part will not be exposed to extremes of heat or cold.[1]

Product Validation Testing:

In the course of the commercial life of the product, several rounds of testing have been conducted, aimed at determining or demonstrating the capabilities and performance envelope of the design.

Three of these tests are noteworthy for purposes of the present problem, given their correspondence to the loading scenarios previously postulated.

1.) Burst test

The most fundamental force a fluid connector must withstand is the force of the fluid media it carries. This test is performed to ensure that the product will be able to withstand pressures far in excess of its rated usage pressure without fracturing. This product was subjected to burst testing at room temperature. The burst pressure for the

[1] In a few instances such as vacation homes which may not be kept air conditioned when not inhabited, higher temperatures are possible. These cases are expected to be outliers, however, and will not be considered in the present analysis.

product in the coupled state was found to be a minimum of 690 PSI. At this pressure, some parts were found to extrude the copper tubing from their compression terminations. No fractures occurred in this testing up to pressures in excess of 1000 PSI.

2.) Tensile test

In order to apply a greater degree of force directly to the area of interest in this problem, the "ears" of the body which retain the clip, parts were exposed to tensile loading. In this test, a steel approximation of the clip is inserted in place of the normal plastic clip. This steel clip has a threaded hole in the center, which is used to apply a linear load with a screw driven load frame.

It was noted in the course of testing the product in this manner that shrinkage voids were present in some parts in the middle of these sections. This feature is worth analyzing in some detail. Figure 4 shows a micrograph of a fractured clip face which has two voids in the ear regions. These voids are found in a significant fraction of these components. Indeed, Voids are a normal feature in injection molded components with sophisticated geometries, and are often (as is the case here) the result of normal cooling of a highly crystalline polymer, such as the acetal used to make this component. These voids are caused by shrinkage related to the volume change the material experiences upon crystallizing and cooling from the molten state during molding.

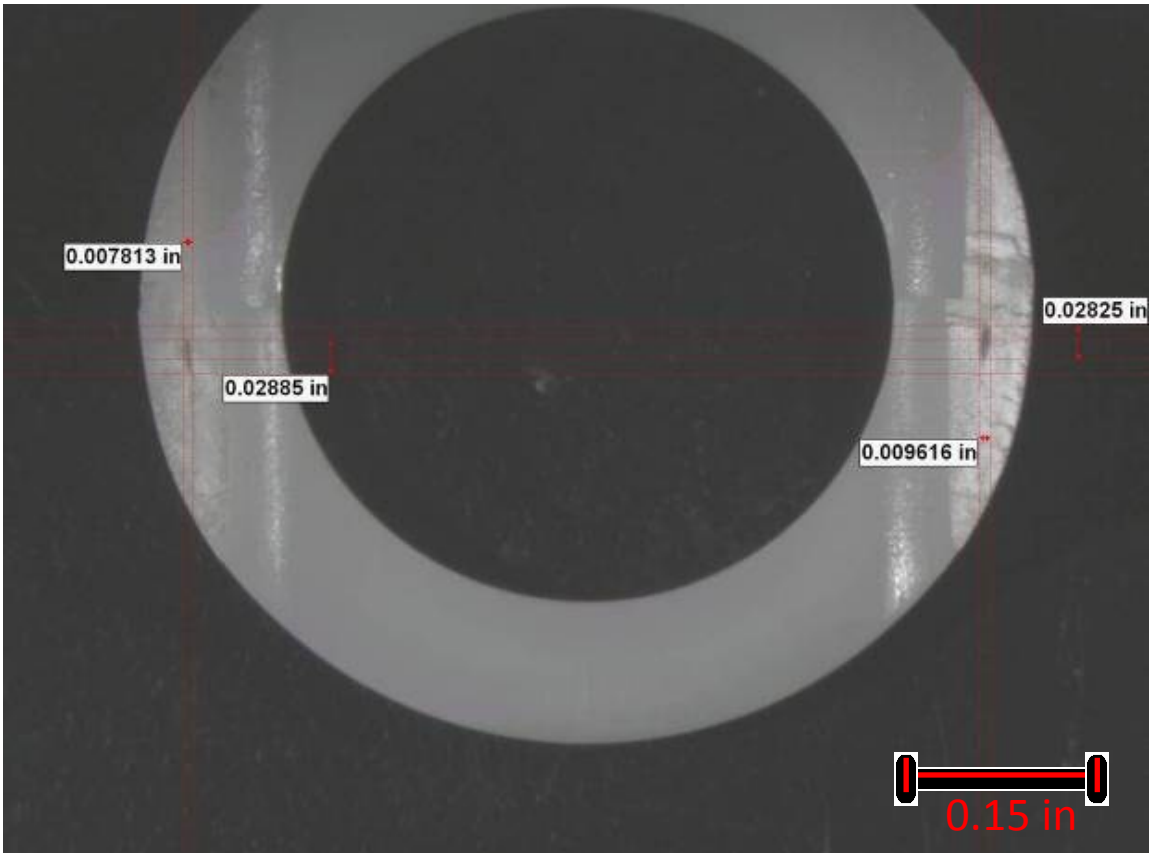

Figure 4: Optical micrograph showing voids in the center of the "ear" cross sections. These voids are caused by shrinkage of the acetal material, and are commonly found in this location. This particular image was captured in analyzing a filter assembly returned for analysis in a lawsuit.

Interestingly, they appear to have little to no effect on the overall strength of the product. Shrinkage voids do not, in themselves, indicate a defective component. Colder's testing and product qualification has demonstrated that a void in this location is common. Further, product validation testing on similar components indicates the

presence or absence of voids in this location does not have a significant effect on part strength, and further, that voids do not predict rupture strength. Test results have indicated no strong relationship between the presence of voids and the force to break parts through the void.

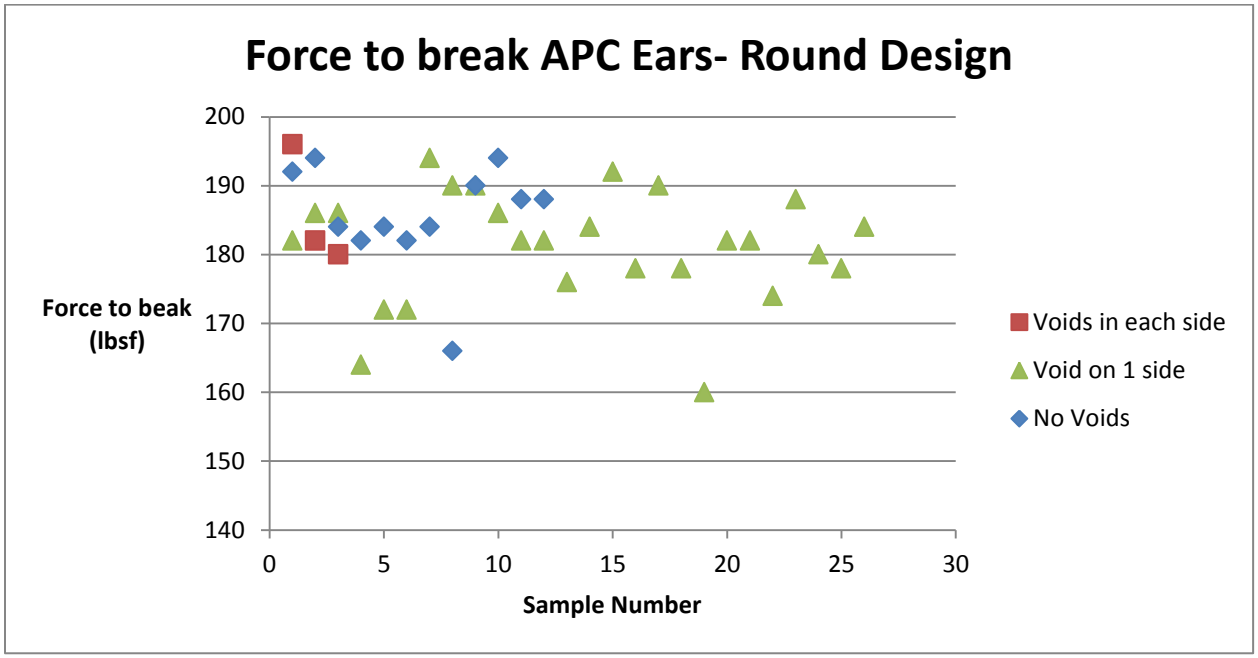

Figure 5: Plot of force to break a part in tensile testing, separated by the presence of voids. Data is shown independently for parts without voids, with voids on the non-gate side, and with voids on both sides of the part.

The insensitivity of force to break to the presence of voids can be understood on the basis of a basic calculation. The dimensions of two typical voids are shown in Figure 4. The area of the voids can be calculated by assuming the

voids to be elliptical and applying the formula A = π a b, where a is half of the long dimension and b is half of the short dimension.

Calculating thusly, the void area is only .000177 square inches on one side and .000213 square inches on the other side. The overall surface area of the fracture is ~.0782 square inches. The void area, then, is 0.4% of the overall surface area. Because stress at failure is given by:

$$\sigma_f = \frac{F_f}{A}$$

A reduction of the load bearing area by such a trivially small amount can be expected to have a trivial effect on the load bearing capacity of the part.

This would not be the case if the void were to act as a stress concentration. However, the experimental data appears to indicate that this is not the case. In the case we are presently analyzing, it was found that the fracture actually appeared to initiate at the end of the ear, not the middle. Crazing and multiple nascent crack initiations were found in that region of the part. Images showing these cracks can be found below.

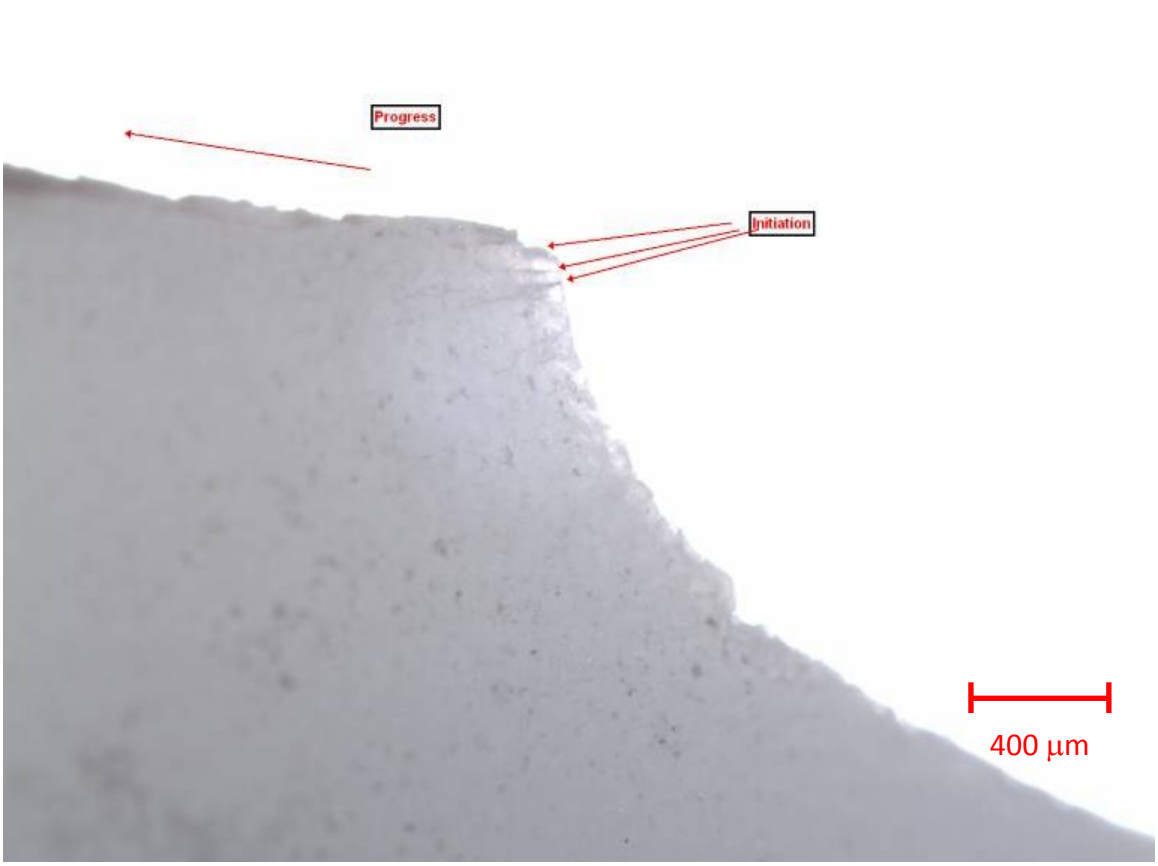

Figure 6: Optical micrograph of the initiation location at the end of the ear. Multiple cracks initiated at this location, one of which progressed across the entire fracture surface. These cracks would not have formed had the crack initiated in the center of the ear near the void, as the overall area when the crack reached this point would have been so small and the effect of the sharpness of the crack tip so large that the material in the plastic zone would simply have fractures, not generated additional, parallel cracks off-plane.

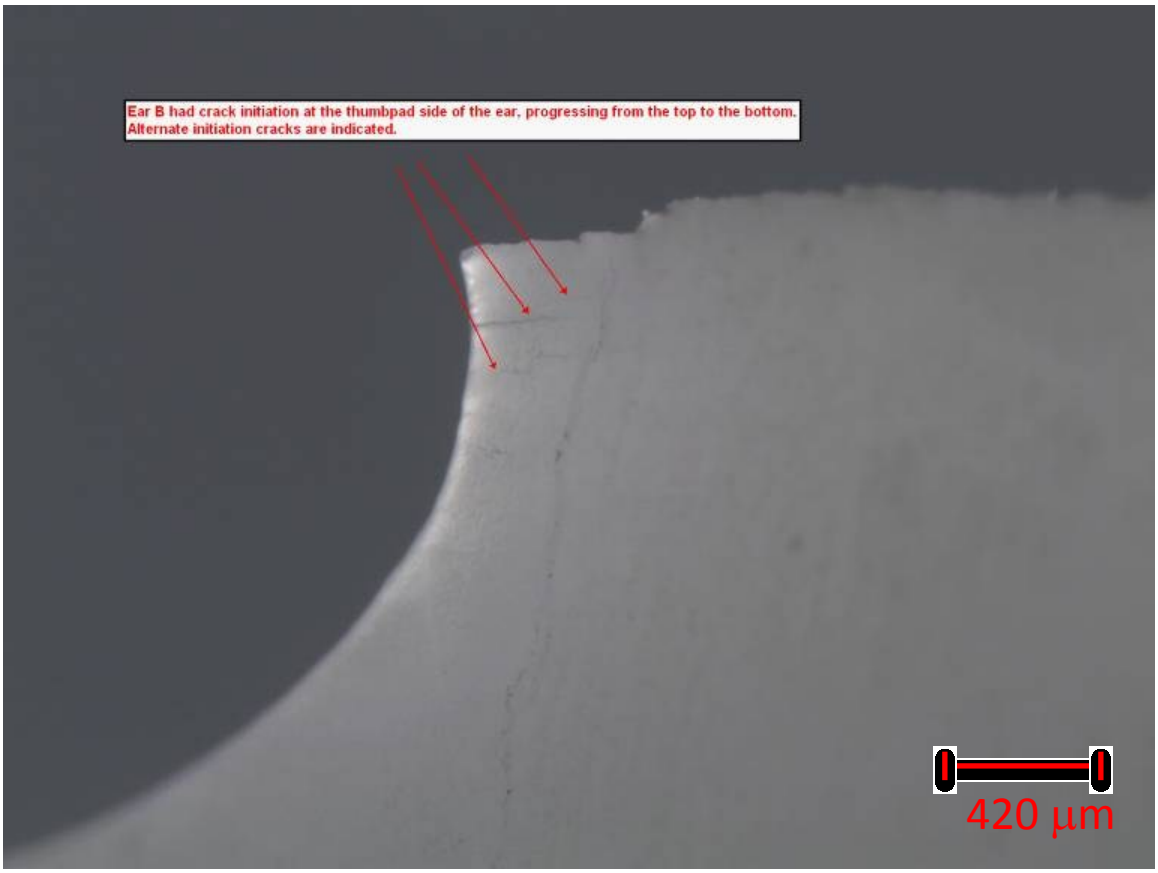

Figure 7: Optical micrograph of the true initiation location at the end of the other ear. Again, multiple cracks are noted. These indicate a relatively uniform state of stress across multiple planes in the material, which would not occur had the plastic material cracked from the center (voids) outward. The crack tip's plastic zone and stress concentration influence would have concentrated stress on the actual fracture plane, not initiated additional cracks near its termination. Further, the vertical stepping seen in this location is not consistent with a rapidly terminating crack, but rather with a "wandering" of a crack between pre-formed crazed regions caused by steady state or fatigue stress.

These cracks near the edges rather than the middle of the ear indicate that the operative stress concentration is not the void in the middle of the ear, but perhaps the relative delicacy of the edge of the ear itself, which concentrates its mass near the center and tapers in thickness to a rounded edge at both top and bottom. The multiple cracks in this location seem to be consistent with images of aggregation of local microcracks in damaged plastics. An image of such a phenomenon is shown in Figure 12.

It seems from this analysis and related observations that the presence of voids is incidental to the mechanism of failure. Further, it is seen that the overall strength of the part in tension is extremely high, requiring a force of over 160 lbsf to generate a failure.

3.) Bending test

While the most fundamental force a coupling will have to withstand is linear, it is not uncommon for parts in real-life applications to be exposed to bending moments. The bending load which can be achieved in this application is large owing to the relatively stiff tubing that is often used as well as the force used to maneuver and position the refrigerator unit, which may be used to pin the filter against unyielding structures such as the back panel of a cabinet or against a wall. Significant attention will be devoted to the magnitude and origin of bending moments in a later section of this paper.

Economic and Legal Considerations:

The reason broken parts are a concern to Colder is because of the liability it is believed to have by insurance companies. When a part breaks in a home, the damage that results is generally covered by homeowner's insurance. The insurance company will often pursue anyone they can identify for their loss in a process called *subrogation.* Because the part at issue has Colder's logo on it, insurers often pursue Colder for these damages despite the fact that Colder is a component supplier to the filter manufacturer, not the designer of the overall system.

Colder relies upon the judgment of the engineers at customer companies to know and determine their own requirements and to ensure that the product they have selected developed does in fact meet those requirements. In most cases, this approach to business is quite successful as the majority of Colder's customers have well defined requirements, and their products are used by sophisticated users who are somewhat technically savvy and skilled at mitigating the risks of potential problems.

The water filter application was one of the first times that a Colder product was marketed on a consumer product where it would be installed and maintained by non-professionals. The product appears to be well suited to the application in most instances as the return rate is less than 1 in 50,000. However, it appears that in some cases a

combination of factors encountered by the couplings is sufficient to cause them to break.

A single broken connector may allow water to escape unchecked, and may result in thousands or tens of thousands of dollars in damages. The component sold by Colder generates only tens of cents in profit. This is not a unique situation for a component manufacturer who supplies products incorporated into more sophisticated assemblies by remote buyers.

Many such cases have been heard and decided upon by the courts. There appears to be a general precedent in most states that the designer of a system is obliged to ensure that the overall system as sold is safe for use:

> It would be unjust and insufficient to impose liability [against a component seller] solely on the ground that the manufacturer of the integrated product utilizes the component in a manner that renders the integrated product defective. Imposing liability would require the component seller to scrutinize another's product which the component seller has no role in developing. This could require the component seller to develop sufficient sophistication to review the decisions of the business entity that is already charged with responsibility for the integrated product.

Restatement (Third) of Torts: Product Liability § 5 cmt. a (1997).

As one court has stated:

> Multi-use component and raw material suppliers should not have to assure the safety [or suitability] of their materials as used in other companies' finished products. First . . . that would require suppliers to

> retain experts in a huge variety of areas in order to determine the possible risks associated with each potential use. A second, related rationale is that finished product manufacturers know exactly what they intend to do with a component or raw material and therefore are in a better position to guarantee that the component or raw material is suitable for the particular applications.

Tellex-Cordova v. Campbell-Hausfeld/Scott Fetzger Co., 28 Cal. Rptr. 3d 744, 747 (2004)

There are many examples of court rulings based on reasoning similar to the above references, where suppliers of a component to an assembly were not held liable for problems with the overall assembly when the component provided was not in itself defective. For example, In *Kealoha vs. DuPont*, 82 F.3d at 900-901 Dupont, the manufacturer of Teflon raw material, was not held for broken dental implants that were made of Teflon because it was only a material supplier. Its material has many uses, was not inherently dangerous, and DuPont was not the entity that chose to specify the material for the implant.

In *Lee v. Butcher Boy*, 169 Cal.App. 3d 375, 386-387 (1985), an electric motor manufacturer was not liable to the plaintiff who was injured by a meat grinder. The plaintiff had claimed the motor should have had an automatic shut off mechanism. However, the motor was a standard, “off the shelf” item incorporated into many different machines by many different manufacturers. It worked properly, and the motor manufacturer did not have input into the design of the meat grinder.

The issue is broadly addressed in *Restatement (Second) on Torts* § 402A cmt. p (1965): "the manufacturer of pig iron, which is capable of a wide variety of uses, is not so likely to be held to strict liability when it turns out to be unsuitable for the child's bicycle into which it is finally made by a remote buyer."

The court in *Kohler Co. v. Marcotte*, 907 So.2d 596 (Fla. Ct. App. 2005), refused to assign liability to a component part manufacturer under facts very similar to those presented in this product situation. Kohler was a manufacturer of small engines, such as the "Magnum 20," sold to original equipment manufacturers ("OEMs") that incorporated them into consumer products designed and assembled by the OEMs, a very similar arrangement to Colder's sale of couplings to OEMs who build them into their own assemblies.

Magnum 20 engines were incorporated into a variety of products, including pressure washers, go carts, generators, and lawn mowers. Kohler sold the Magnum 20 to a company called Magic Circle for use in a riding lawn mower. A lawsuit was filed against Kohler after a 7-year-old boy was permanently injured when his left hand came into contact with a rotating plastic air intake screen on the Magnum 20 engine of a Magic Circle riding lawn mower. The rotating screen was not covered by a protective guard.

Evidence showed Magic Circle knew that a guard was available to cover the entire engine bore housing, including the plastic air intake screen. Magic Circle unilaterally decided not to install the guard, however, because it believed it was not needed. Kohler did not review the design of the lawn mower for safety and did not issue an opinion on the need for a guard.

On those facts, the Court held that Kohler had no liability. The Court noted that

> Kohler designed a generic engine that can be used in various applications. Depending on the particular application and the ultimate placement of the engine in the final product, a guard may or may not be necessary. The engine was not 'defective in itself' and operated exactly as it was designed to operate. As the engine was not defective in itself, it would be unjust to hold Kohler strictly liable where it was Magic Circle who designed the final product, integrated the engine into this product, and determined that a guard was not necessary due to its own design. It only makes sense to place the burden of scrutinizing the final product for safety on the OEM because it is this entity which designed and developed the final product.

Id. at 598.

As in *Kohler,* CPC supplies a component that the filter manufacturer couples with other components to produce a final product. CPC does not have involvement or input into the design, acquisition, or manufacturing of the other parts that make up the water filter kit. Although Kohler made the component that caused the damages – the engine – the court held that it was not liable for that failure because Magic Circle was responsible for making sure the engine was not dangerous or prone to failure within the particular finished product at issue.

Similarly, even in cases where CPC's coupling fractured, CPC properly bears no responsibility because the onus is on the OEM water filter manufacturer to ensure that the coupling will function safely within the finished product without risk of failure due to the use of the finished product in light of the particular demands of the environment in which it will be used.

That said, though legal precedent offers Colder a solid defense, it is not immune from from lawsuits, or even from subrogation claims. The subrogation business is viewed as a strong profit center by insurers, and claims are often pursued on the thinnest of technical or legal justification. The costs involved in responding to cases, even when they are baseless, is still profound.

As a result of the costs of responding to liability claims, the potential liability to profit ratio for the Ametek product is large, and as sales decrease as new generations of filters avoid the need for external connections, that ratio approaches unity. This has created a strong interest within Colder to understand the true cause of the breaks occurring in the field and whether they imply a defective design, as well as being able to identify the mechanism of failure of any given returned component.

Literature Review, Material Properties of Acetal

Acetal history and development

The name *acetal* is rooted in the polymer's linkage of an oxygen atom which joins the repeating molecular unit in an ether rather than ester bond. (Russel B. Akin, 1962, p. 1) Many acetals are possible, as the name does not distinguish the nature of the *mer*. Examples include polyvinyl butyral and polyvinyl formal. (Russel B. Akin, 1962, p. 1) However, in industry, acetal resins generally refer to polyoxymethylene (POM), which is marketed with both homopolymer and copolymer variants (S. J. Barker, 1970, p. 3).

Polymers based on formaldehyde have been known since the late 1850's, when they were first reported by a Russian chemist named Butlerow. The German chemist Staudinger conducted extensive research into addition polymers of formaldehyde in the period between the first and second world wars, and this work was the basis for the production of commercial resins in 1959. (Price, 1970, pp. 1-2)

POM is a polymer based on formaldehyde, CH_2O, or trioxane, its cyclic trimer (Price, 1970, p. 1). The structure of formaldehyde is shown in Figure 8:

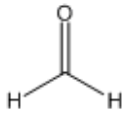

Figure 8: Chemical structure of formaldehyde. (Chemfinder, 2008)

Formaldehyde is produced commercially by the oxidation of methanol or of other hydrocarbons. If hydrocarbons other than methanol are used, additional refining becomes necessary as additional products are produced. (Price, 1970, p. 12) Once formaldehyde is formed, it has a strong propensity to polymerize unless maintained at high temperatures or unless it is mixed with stabilizers. (Price, 1970) Formaldehyde has many applications, including cleaners, disinfectants, explosives, cosmetics and fertilizers, in addition to its use in resin production. (Price, 1970)

(Price, 1970, p. 12)

The gap between the early work on formaldehyde polymers and the development of a useful commercial resin is generally traced to the difficulty in obtaining formaldehyde of sufficient purity to produce chains of appropriate length, and with the difficulty of stabilizing those chains to prevent depolymerization once they had been formed. (S. J. Barker, 1970, p. 22)

POM acetal (which will in this work be refered to interchangeably as either POM, the correct polymer name, or as Delrin, the commercial name for the material actually used in the product, or simply as acetal, as it is known generically in the plastics industry (Price, 1970, p. 1).) is a material with long, unbranched polymer chains that crystallize well upon cooling from a molten state, and have high degrees of stiffness, toughness and chemical resistance. (Russel B. Akin, 1962, p. 2) The unbranched chains crystallize to an uncommon extent- homopolymer acetal has crystallinity between 75-85% depending upon thermal history. (C. F. Hammer, 1959, p. 172)

Acetal resins were first commercially introduced in 1956, commercial scale production began in 1959, and a copolymer version was introduced by the Celanese Corporation in the early 1960s. Commercial scale production occurred in 1959, and a variety of papers written by scientists at Dupont were published that same year. Several patents were granted related to the production and chemistry of the new material, however, the Celanese Corporation nevertheless released their own version of the acetal material, in copolymer form, in 1960. (Price, 1970, pp. 1-2)

The version of POM developed by Dupont, marketed with the tradename Delrin, is shown below in Figure 9.

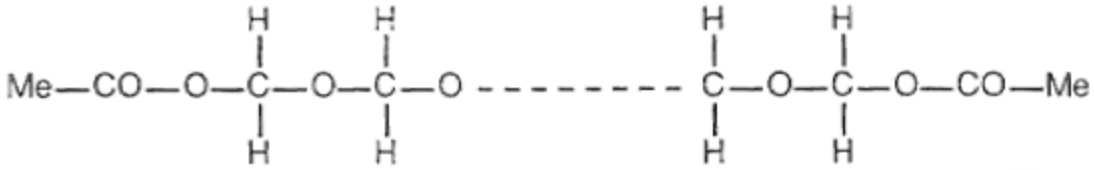

Figure 9: The chemical structure of homopolymer acetal- note the regularly repeating C-O bond along the chain, terminated in methyl groups. Image from (Patel, 1993, p. 46).

The structure of the copolymer variant is shown in Figure 10.

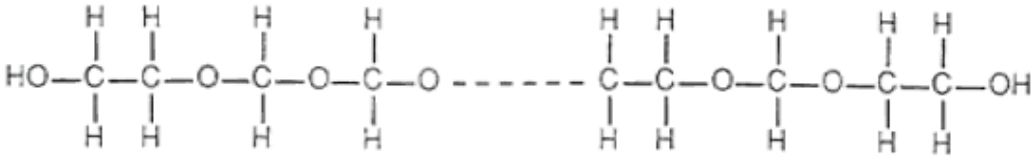

Figure 10: Schematic of the chemical structure of acetal copolymer. Note the presence of C-C bonds; these can act to arrest polymer degradation, given the higher enthalpy of the C-C bond. Image from (Patel, 1993, p. 46).

The difference between acetal copolymers, like Celcon and Hostaform and homopolymers like Delrin lies in the chemical structure of the polymer chain. The homopolymer backbone is comprised entirely of C-O bonds, with little to no polymer branching. The copolymer, however, contains some C-C bonds while remaining unbranched. The addition of C-C bonds, which are more chemically stable than C-O bonds, results in a material with slightly better chemical resistance and better resistance to thermal degradation, as the C-C bonds serve to arrest chain cleavage caused by

several different solvents and heat events. This difference also offers processing improvements as well as property improvements for molded articles.

However, the non-regularity in the makeup of the polymer backbone prevents the same degree of crystallization as in the homopolymer variant. As a result, the homopolymer has greater short term strength and rigidity as well as a higher melt temperature and softening point. As a result of these different structures, there are differences in properties between the two chemistries, however, those differences are fairly small. (Price, 1970, pp. 9-10)

Table 2: Properties data for two commercial grades of acetal resin, one homopolymer and the other copolymer. The homopolymer represented here is Dupont Delrin® 500P BK602 and the copolymer is Ticona Celcon M90™.

Property	Copolymer	Homopolymer
Elongation at Yield	10%	14%
Method	ISO527	ISO527
Yield Strength	9570 PSI	10,300 PSI
Method	ISO527	ISO527
Elongation at break	n/a	25%
Method	n/a	ISO527
Tensile Modulus	400ksi	450 ksi
Method	ISO527	ISO527
Heat Deflection Temperature (264 PSI)	214F	205F
Method	ISO75-1/-2	ISO75-1/-2
Notched impact (izod)	5.7 kJ/m^2	8.0 kJ/m^2
(Room temp)	ISO180/1A	ISO180/1A
Unnotched impact (Charpy)	188 kJ/m^2	180 kJ/m^2
(Room temp)	ISO179/1eU	ISO179/1eU

(Ticona/Celanese Corporation, 2009) (Dupont Engineering Polymers, 2006)

Acetal is considered one of the 'engineering plastics.' This is a term often bandied about in industry with a vague meaning. One of the better precise definitions found in the literature is the following:

Engineering plastics are those which:

a.) Are among the strongest of thermoplastic materials, where the term "strong" refers to the following physical properties over a wide temperature range: High Young's modulus, low creep under load, and high mechanical strength under conditions of both steady applied loads and sudden impact loads.

b.) Their physical properties have been thoroughly evaluated and are presented in a form acceptable as design data for engineers.

c.) They find their major markets in the field of mechanical engineering, replacing other materials, usually metal, in load bearing applications

(Price, 1970, pp. 6-7)

This delineates acetal from commodity resins, which may have inferior properties, but are nevertheless suitable for less demanding applications.

From the earliest uses in the first two years after commercial availability of the first POM resin, the material found wide use in applications as diverse as bearings (replacing

steel), fan blades (replacing steel), drive sprockets in agricultural equipment (replacing cast iron) and sliding surface carriers in copy machines. In addition to these applications, early literature indicates that from the very introduction of the resin it has been used in plumbing fixtures, from water softener valves to pump housings and impellers to swimming pool treatment systems. (Russel B. Akin, 1962, pp. 169-174) In the late 1960s, roughly 14% of the 18,500 ton annual usage of acetal was used in the plumbing marketplace.

Material Characteristics, Processing, and Shortcomings

Key properties for the resin include its combination of strength and temperature resistance even in wet environments where nylons would be unsuitable, and the excellent creep and chemical resistance properties that polycarbonate lacks due to its amorphous structure. These were key advantages of the material early in its lifecycle. (Russel B. Akin, 1962, p. 6).

These properties are related to the uniquely high crystallinity of the material. The volume fraction of crystalline material in acetal is particularly high (~80%). This is responsible for several notable properties:

1.) Resistance to chemicals: There are no solvents for acetal at room temperature, and very few at temperatures up to 100C. Further, when the polymer itself dissolves liquids, the entire volume of liquid is contained in the amorphous regions of the material due to the high enthalpy involved in the crystallization process. (R. G. Alsup, 1959)

2.) Friction and Wear Characteristics: Acetal has a very low coefficient of friction and good wear characteristics. The wear of acetal gears is extremely low even against metal mating gears unless the gearset is run at speeds and contact pressures sufficient to cause heating to the melting point of the acetal. (K. Mao, 2006) This has made acetal it a popular resin in gear applications such as

window carrier assemblies, washing machine drive assemblies, and low-cost bearings.

The material's high crystallinity means that there are few amorphous regions (with their relatively loosely coiled polymer chains) at the surface, which gives the material a harder, more lubricous surface.

3.) High operating temperature: The melting temperature of homopolymer acetal resins is approximately 175-180C, with some melting of very small or otherwise unstable crystalline regions beginning around 125C, as evidenced by heat capacity changes. (Goodman, 1959) This is significantly higher than many other widely used polymers, such as polycarbonates and nylons, and enables acetal to be used in higher temperature applications than many resins of similar cost.

4.) Deflection at Yield: Acetal has a truly impressive yield strain- while it does vary somewhat depending upon grade, it is typically in the range of 12-20%. (Dupont Engineering Polymers, 2006) This has caused the material to be touted as "the spring steel of the plastics world." This resilience under deformation is an asset in applications where significant mechanical displacement is likely (strain-controlled applications) such as screw threads, and has caused it to be a favorite at Colder because it does not suffer from excessive stress relaxation when tightened into place in a rigid mounting.

These properties are some of the most advantageous, especially given acetal's relatively low cost (typically ~$3/lb at high volume.)

Some of the drawbacks of the material include its high shrink (1.9%) (Dupont Engineering Polymers, 2006), which can lead to void formation. The amount of shrink is due predominantly to the large volume change on crystallization from the melt. This also requires molds to be designed to allow large amounts of material to be injected into the mold after the initial fill, to continue packing the tool with fresh molten resin to prevent void formation. This puts some limitations on designs, and can require multiple gates for some geometries to be manufacturable.

Acetal also shares the characteristics of other crystalline materials in that it may warp or deflect at high temperatures due to annealing effects, and its crystallinity may lead some molders to "torture" the process in order to produce parts in specification while sacrificing material properties. As such, the processes and properties of acetal should be monitored more carefully than other resins may require so as to ensure that the parts remain consistent over time.

Injection molding and extrusion grades are available, and blow and rotational molded articles are also made from acetal. The APC product as issue in this analysis is injection

molded. The processing windows are comfortable, and the recommended process parameters are shown in Table 3.

Table 3: Recommended Processing Parameters for Delrin 500P acetal. (Dupont Engineering Polymers)

Parameter	Minimum Recommended	Maximum Recommended
Melt Temperature	210C	220C
Melt Temperature (Optimum)	215C	215C
Mold Temperature Range	80C	100C
Mold Temperature Optimum	90	90
Processing Moisture Content	<.2%	<.2%
Hold Pressure	80 MPa	100 MPa

In regard to fracture properties, Delrin's impact resistance varies relatively little with changes in temperature, however, the unnotched Izod impact strength is greater than the notched Izod impact strength, which indicates that designs incorporating acetal should be designed to maximize corner radii. (Russel B. Akin, 1962, p. 7)

Fatigue of Acetal

Fatigue is a common failure mode for both metals and plastics. It occurs when cyclic stresses of less than the yield or ultimate strength of a material cause the nucleation and/or the advance of a crack. However, metal and polymer fatigue are different in that different mechanisms are responsible in each material class. In metals, fatigue may operate through the advance of dislocations through the material, and crystal structure has a significant bearing on the fatigue characteristics of the material. In semi

crystalline plastics, dislocations do exist in that there is such a defect in polymer crystals, but dislocation motion is not responsible for fatigue because polymers lacks metallic bonding, which is required for dislocation motion. Instead, in plastics, fatigue is often related either to heat generated through mechanical hysteresis or due to material damage, such as chain cleavage or pullout.

A further distinction from metal fatigue can be drawn in that, for metals, a significant portion of the fatigue life is spent in crack progression. That is, stable crack progression accounts for a substantial period of the products' useful life. For plastics, crack propagation is often a much smaller portion of the overall life of the product. Therefore, many of the key insights of fracture mechanics, which is largely concerned with the mechanics governing the advancing crack may be of little use for plastics if the majority of the damage to the material occurs before the crack becomes apparent. In many cases, the process of crack initiation may consume 95% of the fatigue life of polymers. (Roel P. M. Janssen, 2008)

Early research into the fatigue of polymers in general, and acetal in particular, made clear that the mechanisms responsible for fatigue were different between polymers and metals. The loss compliance, a measurement of the internal damping characteristics of polymers was of particular interest (M.N. Riddell, 1966). This material parameter, defined as the ratio of the strain 90 degrees out of phase with the applied stress

compared to the applied stress, served as a predictor of whether a material would have an endurance limit. Loss compliance, in effect, is a measurement of the amount of energy created by the applied stress. Early efforts indicated that the variance of loss compliance with temperature and the tendency to create local minima at different temperatures was responsible for whether a polymer would display an endurance limit or not.

Thermal Fatigue:

Schematically, for heat dominated fatigue (typically at high frequency), the strain of the material in response to applied stress generates heat. The generation of heat tends to soften the material and increase its loss compliance. For some polymers, this increase in loss compliance with temperature is monotonic. For these materials, continued straining will continually increase the temperature of the material which will continually lower the loss compliance, leading to a vicious circle. Such materials will fail by thermal fatigue, as the damping of the material is capable of heating the material through its glass transition temperature. For other polymers, the loss compliance is not monotonic, and local minima may exist. In a local minimum the strain heating will result in a reduction in loss compliance and an equilibrium may be established. Such materials, (e.g. PMMA, TFE) display endurance limits.

In this application thermal fatigue is unlikely to play a role for several reasons. First, the application temperature is far below T_m for POM (352°F (Dupont Engineering Polymers, 2006)). Second, the sources of possible fatigue loading are not high frequency phenomena. The only events which may cause such loads are physical handling from installation (~once every six months), water hammer from the refrigerator (~ten times per day), and water hammer from other fixtures (~thirty times per day). These events are too widely dispersed in time to allow significant heat buildup. Third, the part is kept in a temperature moderated environment. Again, this limits the ability of heat to build up and affect the material. Fourth, the manufacturer's data indicates that the material specified has a 10^6 cycle endurance limit at 5,000 PSI, indicating that it is not especially sensitive to fatigue stresses.

Mechanical Fatigue

If fatigue is a significant issue for the product, the parameters of the application indicate that it would not be thermal fatigue, but rather the type of fatigue caused by mechanical damage to the microstructure of the material. Rather than being rooted in local melting of the plastic, physical damage fatigue is rooted in damage to the microstructure.

Broadly, it is known that mechanical damage related fatigue does occur. The state of the literature in dealing with such damage is not tremendously far advanced. In particular, the early stages of such fatigue cracks is poorly understood. At the

nanometer size regime, the cracking process is likely a blur between chemical reactions and conventional crack propagation. Theoretically, the picture of a homogeneous body under stress has been used, with chemical bonds breaking in random locations. Stochastically, some regions of material will experience higher levels of bond-breaking, which increases stress in those areas, resulting ultimately in the creation of submicrocracks or crazes. (Zhurkov S.N., 1969) The bond-breaking portion of this regime appears to have eluded observation to this point in time, however, a notable paper (Jones & Lesser, 1998) has observed the initial distribution of submicrocrazes, and their progression into microcracks and crazes, whereupon a Paris law relationship appears to prevail.

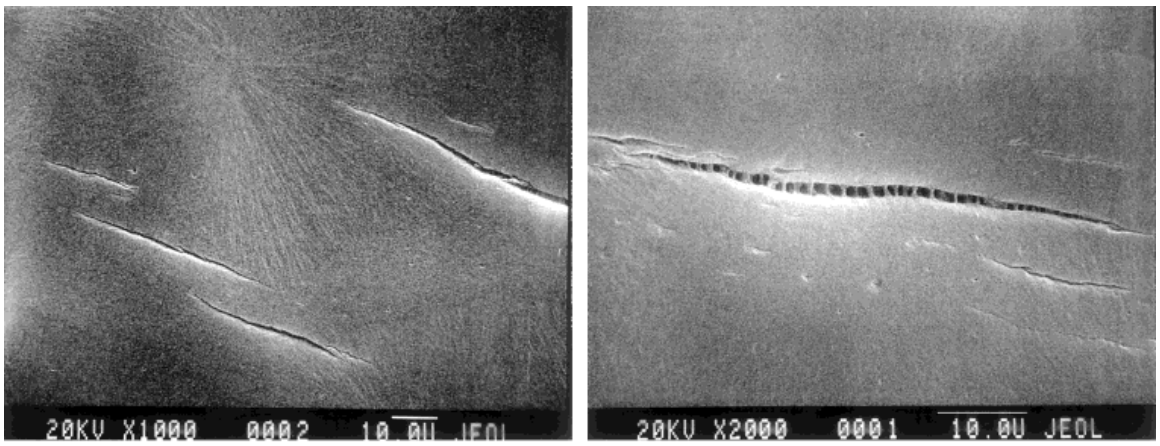

Figure 11: Scanning electron micrographs showing fatigue-induced crazes in polypropylene. Both polypropylene and acetal are semi-crystalline polymers, so analogous behavior is likely. The samples have been prepared and etched to reveal spherultitic structure. Note that the crazes do not orient with respect to spherultic features. (Jones & Lesser, 1998).

After initial coalescence of broken bonds into crazes, crazes themselves accumulate, and ultimately coalesce themselves into larger crazes and cracks. Throughout this process, it appears that spherulitic morphology has limited effects- the cracks and crazes form with orientations determined by the stress on the sample rather than the orientation of the spherulitic lamellae (see images in Figure 11.)

Under creep loading the formation of microcracks and crazes appears to accumulate to a saturation level which is independent of load until final fracture. Further, the kinetics of the accumulation of these defects appears to be closely related to creep kinetics. (Zhurkov S.N., 1969) In fatigue loading, a similar damage phenomenon appears to occur, with crazes in isotactic polypropylene coalescing into larger crazes. Further, the tip of the craze region is an area of stress concentration, which tends to facilitate craze growth upon further loading, as well as initiate crazes on adjacent planes in the local material. (Jones & Lesser, 1998). This indicates a similarity between the creep and fatigue failure modes and implies discerning between the two is not straightforward because both result in the same kind of material damage.

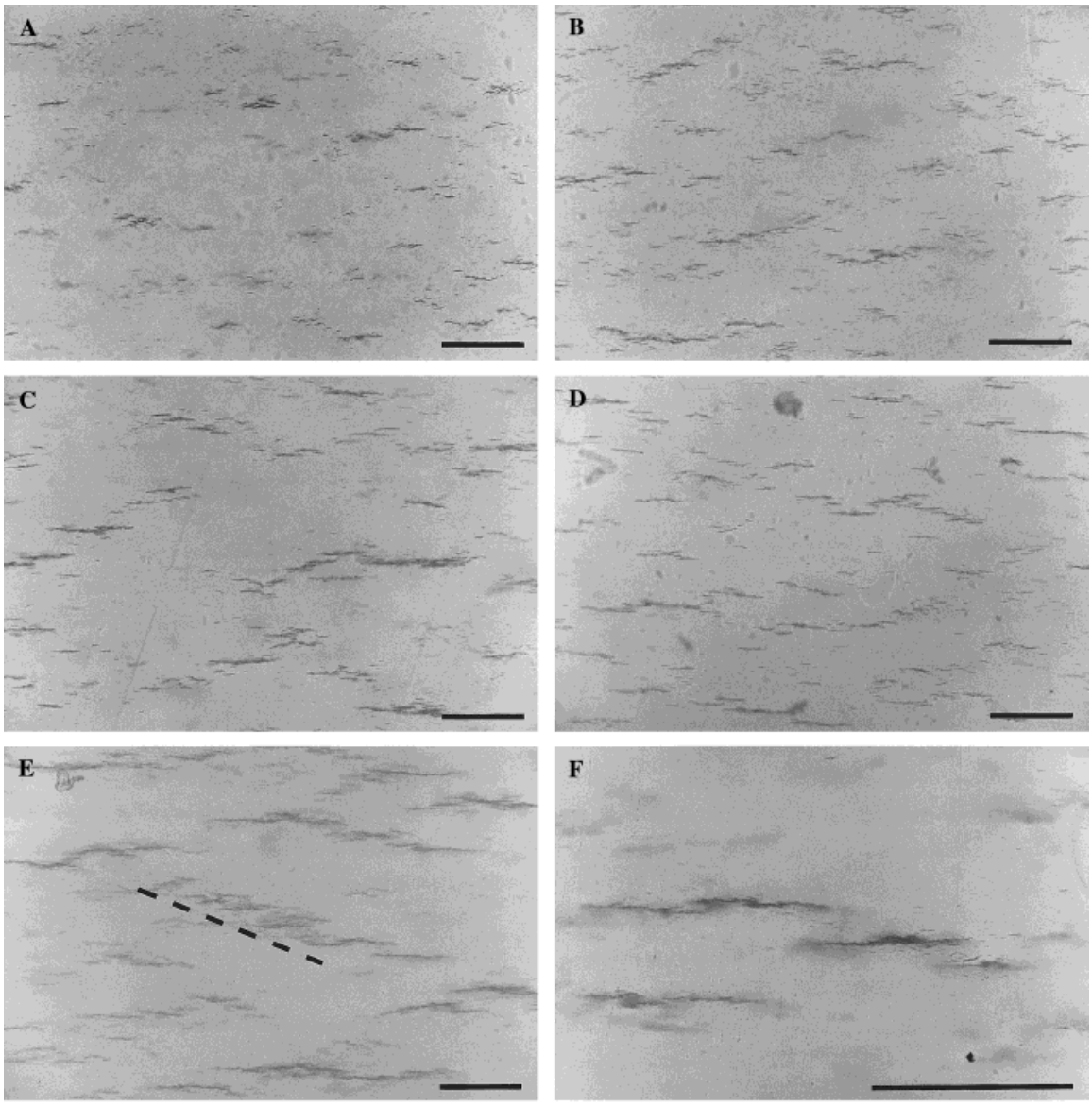

Figure 12: Transmission optical micrographs at different cycle counts. Image A taken at 10^5 cycles, B at 2 x10^5 cycles, C at 4 x 10^5 cycles, and D at 6 x 10^5 cycles. Image E was taken at 10^6 cycles, with dashed line highlighting coalescence of adjacent crazes. Image F was taken at 6 x 10^5 but at higher magnification showing stress interaction between crazes. Scale bars indicate 100 um. All originated in (Jones & Lesser, 1998).

Creep of Acetal

Polymer creep is the result of the viscoelastic nature of polymers. In amorphous materials like polycarbonate and polysulfone, the phenomenon of fatigue can be understood in terms of chain slippage and disentanglement. In the case of

semicrystalline materials such as acetal, creep must be understood in a way that captures the effect of the crystalline regions of the material, and how that differs from the effect of the amorphous regions.

For the purposes of creep, a semicrystalline polymer can be viewed as a two phase system, almost like a composite (Schultz J. , 1984). The nature of the composite structure varies considerably with processing. In particular, the thermal history and flow characteristics of the molten material have a significant impact. Both of these sets of variables are related to mold design for the specific part being considered. Generically, however, this structure can be most easily understood in terms of distance from the walls of the mold used to produce the part.

First, it is important to note that the mold walls are generally much cooler than the plastic resin being injected. As plastic fills the mold, the material which flows out from the melt front and makes contact with the mold wall begins to cool very quickly, and this cooling effect causes rapid crystallization at many, many sites. Further, the flow of molten material generates shear, which causes fibril nucleation parallel to the flow direction. This leads to a uniform crystal orientation in the material at this depth. (S.S. Kati, 1982) So many crystals are created that growth along the plane of the mold surface is extremely limited. The only direction with amorphous material available for

crystal growth is “down,” toward the still hot, molten material in the cavity of the mold. This results in a highly oriented skin near the surface of the mold.

Deeper in the wall section, continued growth downward of the material in the skin occurs. Fresh melt continues to flow past the frozen skin to fill the remainder of the cavity and this material is above the glass transition temperature and does not immediately crystallize. As the cavity fills and this flow of fresh molten material stops, the molten material begins to cool and crystal lamellae from the skin are able to grow into this region. However, the absence of flow at this point in the injection cycle removes the cause of the orientation effect seen when the skin was forming. The crystal structure in this portion of the section retains the growth direction of the skin (downward) but will have the normal twist of a polymer lamellae. Full sphereulites do not develop in this region, which is a transition region between the highly oriented skin on the surface and a more isotropic mass of material near the core. This transition region is called the “transcrystalline” region of the section.

The third region of the wall section is in the core of the material. Here, crystallites may nucleate spontaneously, forming full spherulites. In this region, spherulite growth is competitive with growth from the transcrystalline region. The three regions are shown schematically in Figure 13.

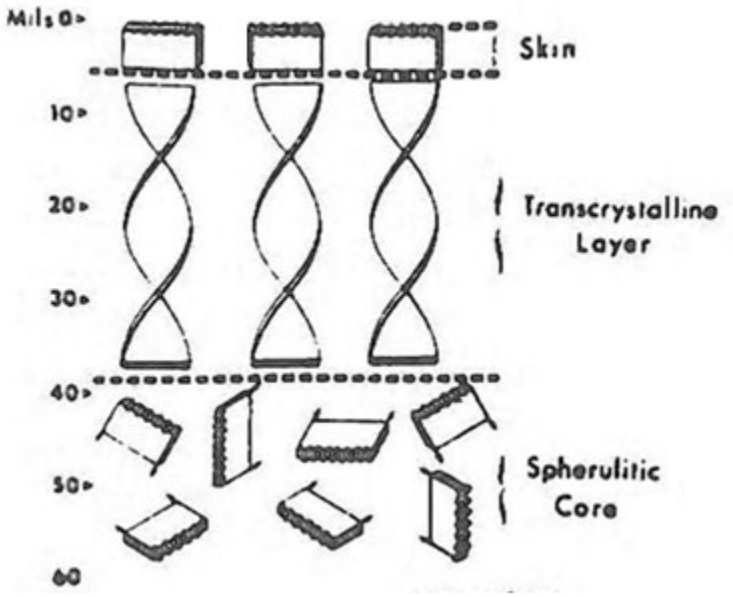

Figure 13: Image showing the three regions in an injection molded semicrystalline polymer. From (S.S. Kati, 1982).

The local structure is different in each of the three regions. However, in each of them, both amorphous and crystalline material is found. Further, unlike in other two-phase systems such as precipitation hardened metals, the two phases do not only bond at phase interfaces, but there are a number of continuous polymer molecules bridging between the crystalline and amorphous regions. (Schultz J. , 1984) Upon straining, these molecules may do three different things:

1.) Break

2.) Be drawn out of the crystal(s) they are a part of, creating fibers

3.) Cause shear failure of the crystal(s) they are a part of

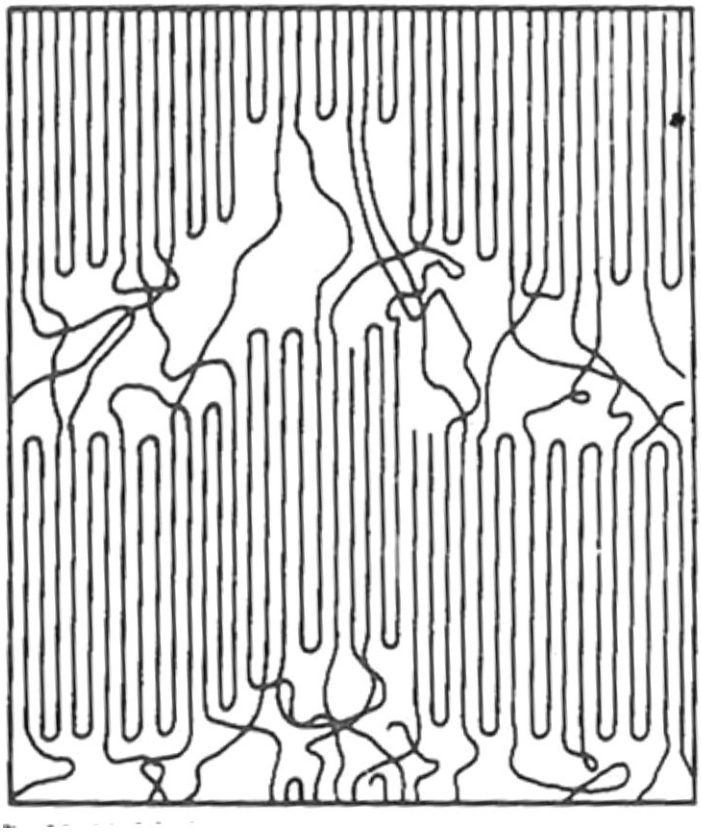

Figure 14: Graphic showing two spherulites and the amorphous region between them. As drawn, a load in the vertical axis is shifting the lamellae, breaking up the structure of the spherulites. (J. Schultz, 1984)

The behavior which dominates appears to vary with the number of bridging molecules present in a sample. When few molecules tie the different regions together, the load is concentrated over a smaller number of bonds, and breakage is more likely. When incrementally more molecules are present, sufficient stress may exist to draw material from the individual lamellae in a spherulite.

An example of the drawing effect in a thin film specimen of POM is shown in Figure 15. This image shows the effect of drawing a multilayered POM crystalline film. (Gohil, Patel, & Patel, 1974). This experiment demonstrated that deformation can cause bridging chains between two crystal arrays to draw material out of the crystals to accommodate deformation of the bulk.

Figure 15: A crystal multilayered from spiral growth was fractured through deformation of 100% in the direction indicated by the arrow. (Gohil, Patel, & Patel, 1974)

When yet more bridging molecules are present, rather than causing the drawing out of material, the strength of the polymer backbone connection between spherulites, or between spherulites and the amorphous state may be stronger than the crystalline interactions holding the lamellae in place within the spherulite. This can cause crystalline material to deform or shift within the spherulite. (Schultz J. , 1984) A graphic showing this concept is shown in Figure 14, and in fact this type of fracture can be seen along with fibril generation in Figure 15.

In both creep and fatigue all three mechanisms may be active. Which predominates appears to be influenced by thermal history, load rate, load magnitude, and temperature, among other variables. In this application, all but the thermal history of the components is uncontrolled and unknown, further complicating the present analysis.

Because the result of both creep and fatigue is to generate microcrazes and cracks, it is to be expected that there is some interaction or overlap between the two phenomena, with both mechanisms ultimately entangling under some loading conditions. The relationship between time and loading for viscoelastic materials makes the two damage mechanisms difficult to disentangle for polymeric materials. It can therefore be difficult to determine which kind of loading was responsible for a given part failure after the fact if the load condition is unknown. Yet, being able to determine if a part failed due to

creep loading or fatigue loading would be very valuable for forensic failure analysis. In order to discern between mechanisms, parts with known load histories were fractured and their surface morphologies analyzed by SEM. This work is discussed in more detail in the fractography section.

Loads In Service

When the coupling is in service, several sources of loading are possible. These sources include mechanical bending, internal pressure, and mechanical tension. In order to determine which mode of failure may be operative on the part, it is useful to analyze each potential load source in order to determine the state of stress the part may experience in service.

Working Pressure:

The maximum rated pressure for the APC series connectors is 125 PSI. The maximum rating of the filters used in this application is lower- 80 PSI, due to the limitations of plumbing codes.

This fluid pressure acts to separate the insert and body portions of the coupling. The two components are held mated together by the clip (thumblatch), which secures an insert to the body, transferring any pressure related forces to the body ears which retain it. It is these ears which break in the cases being considered in this analysis, which makes the effect of pressure an important parameter to consider.

In order to determine the effect of typical pressures on the connector, FEA analysis using the Algor V. 23.1 software was performed. Both 40 PSI and 80 PSI equivalent forces (7.2 and 14.4 lbs) were applied to a simplified APC body component to determine the stress in the clip ears. Output from the analyses is show below. Note that these

analyses were conducted using elastic simulation only, resulting in higher than actual stresses. Note also that all FEA images use the same stress scale, shown in expanded form in Figure 16.

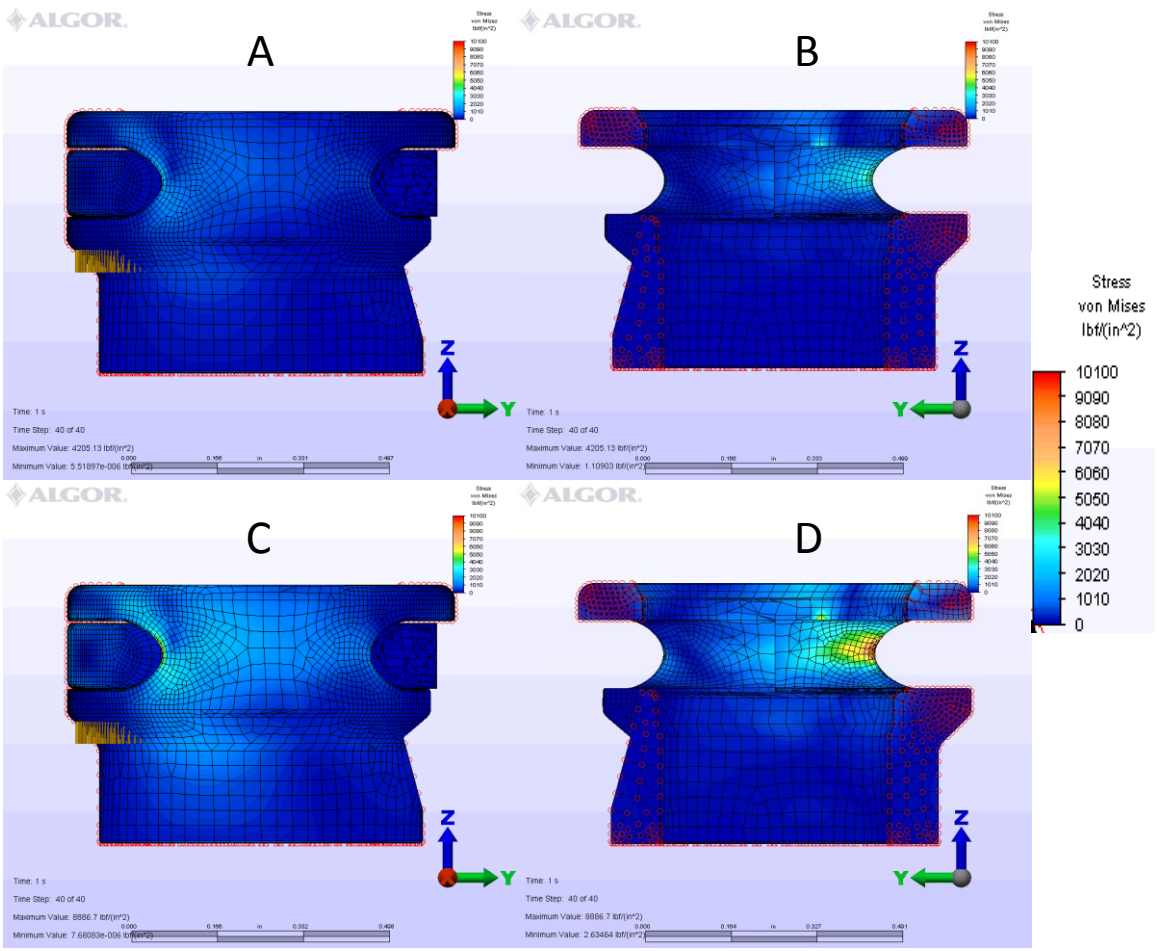

Figure 16: FEA analysis of the connector. Frame A shows a 40 PSI simulation. Frame B shows a 40 PSI simulation from the interior of the clip slot, with the clip suppressed to allow a view of the stressed material. Frame C shows the same part with an 80 PSI simulated pressure. Frame D shows the 80 PSI simulation from the interior of the clip slot, with the clip suppressed to allow a view of the stressed material. All frames use the same color scale for stress, expanded to the right side of the figure.

Water Hammer:

As calculated above, the maximum possible pressure the filter assembly could encounter due to water hammer effects would be 385 PSI. This level of pressure was also simulated using the Algor package. Results are shown below. Note however, that this pressure would be mitigated by the presence of the filter housing and its ability to absorb volumetric fluctuations caused by water hammer. Indeed, in its own testing General Electric, one of the filter manufacturers, performed water hammer testing on samples of these parts, and they were found to pass. Given the limitations of the simulation, it is possible that the stresses calculated above are simply inaccurate. However, they may still be of use in terms of enabling a comparison of the different loading scenarios, even if the absolute results do not agree with experiment.

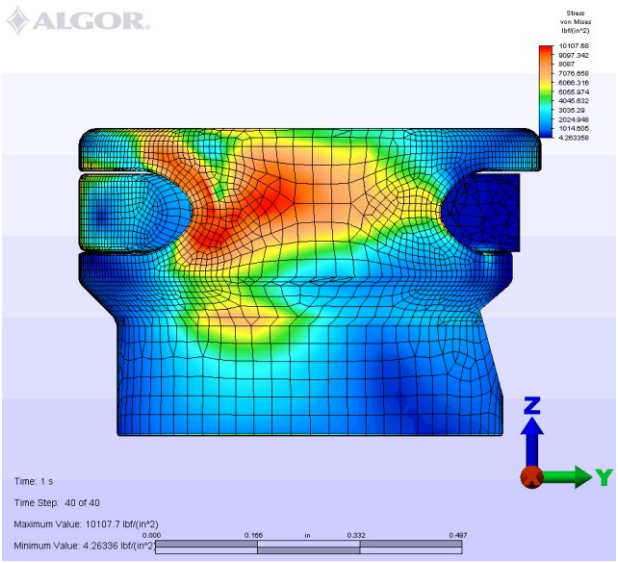

Figure 17: Simulated effect of water hammer to 385 PSI pressure.

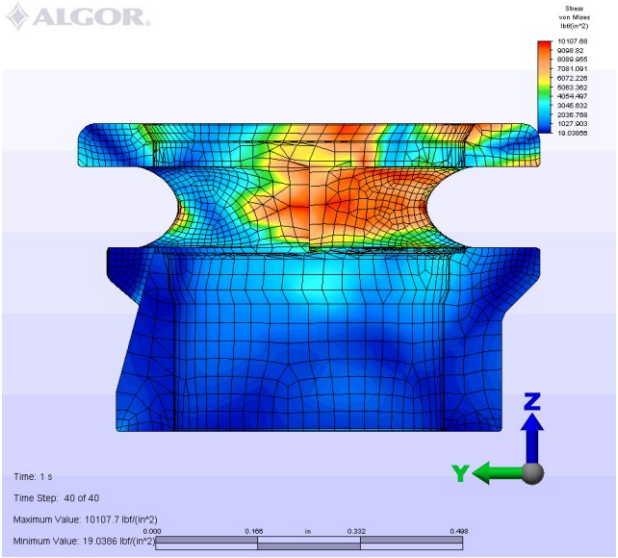

Figure 18: Simulated effect of water pressure to 385 PSI. Clip suppressed to allow view of stress levels at interior surfaces.

These FEA analyses must be interpreted in light of experimental data, such as that reviewed in Figure 5, which showed that the parts analyzed can bear a load of ~ 160-195 lbsf before failure occurs in a short term test. Long term testing has shown no evidence of cracking despite three months of loading at 60 pounds of force. The 80 PSI simulation shown above was conducted with a load of 14.4 pounds (calculated pressure:force equivalence based on cross sectional area and hydraulic pressure) and shows a stress approaching 7000 PSI at the bottom of the ear, where fracture is expected to begin. This is ~70% of the published yield strength of the Delrin material used to make the part. The water hammer analysis shows considerable portions of the ears at high levels of stress, but experimental results have shown that these parts take 2-4 times the simulated pressure load before failure occurs. Because experimental evidence shows that loads up to ~14x larger than the simulated load are required to break the part, it is clear that the simulation is not closely correlated with reality and are not suitable for a meaningful or accurate engineering analysis of the part design. The departure between the simulation and reality is likely rooted in the elasticity model used in the solver, the complex geometry of the part at the location of maximum stress, inaccuracies in the way the load is transferred by the software from the clip to the ear, and the absence of the insert half of the connection in the model.

These simulations may be useful for comparisons between different load conditions, but cannot be relied upon for an accurate understanding of real stresses in the part at any given load level. They will be used to compare the effects of pressure and water hammer to bending moments only, and no absolute values of maximum loads or stresses should be inferred based upon the above comments.

Bending Moments:

The use of copper tubing with the water filter offers an opportunity for additional stress. While both copper and polyethylene tubing can be used in filter installations, the use of copper appears most common in returned assemblies. The compression fitting used to mate either type of tubing works by inserting the tubing into the termination of the coupling, then using a threaded nut to compress a ferrule between the tubing and the inner diameter of the thread wall. Figure 19 shows how compression joints are assembled.

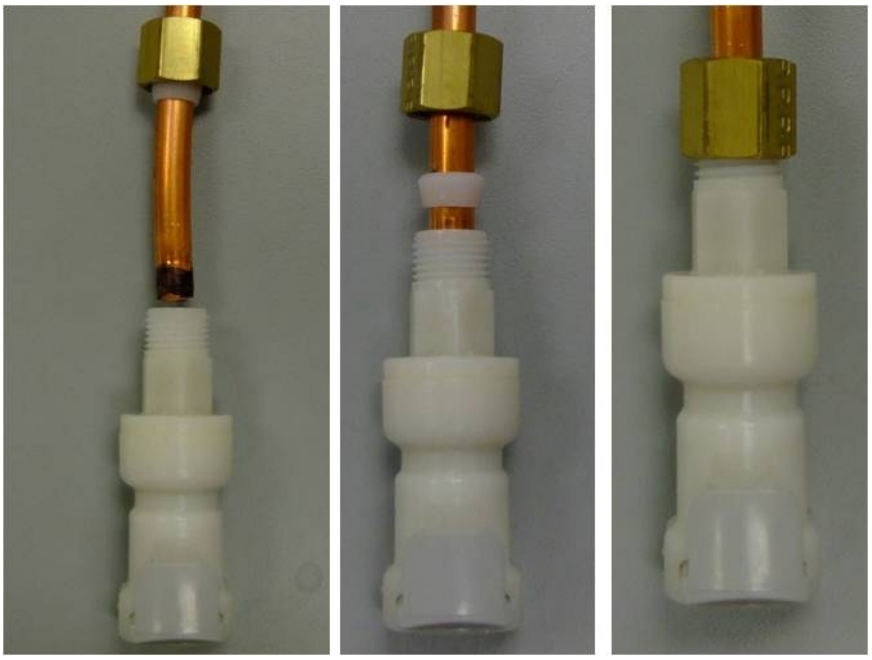

Figure 19: The three stages of tubing installation into a compression termination. The copper tubing is inserted into the termination (note the disappearance of the black region) and a soft plastic ferrule is compressed between the tubing and the inner wall of the termination, forming a seal.

The rigidity of the copper tubing allows the transfer of mechanical loads to the coupling. A large proportion of returned parts show evidence of cracking in the thread region. It is believed that these cracks are caused by bending moments transferred to the plastic by the copper tubing inserted into the ID. A bending moment applied thusly would result in a significant hoop stress at the edge of the plastic thread. Indeed, the cracking observed is confined to one side of the thread in all cases, which appears consistent with such a loading scheme. The only likely alternative explanation for the cracking is general overightening of the joint, however, were this the cause, the cracking would be expected to occur uniformly around the circumference, and not only along an ~180 degree arc. Figure 20 shows an optical micrograph of the termination cracking phenomenon.

Earlier, the effect of water hammer was mentioned as a possible cause of breakage. These fractures, while they are not associated with loss events, provide evidence that water hammer is not a factor. This region of the part is relatively insensitive to pressure. While the ears may be stressed significantly as pressure spikes act to separate the insert and body halves of the connection, this region is relatively unaffected, yet fractures anyway in a large number of losses. Further, no such fractures have been observed in the larger diameter wall sections of the body or insert components despite their geometrically larger pressure sensitivity. Were water hammer a dominant cause, this associated fracture mode in the thread ought to be accompanied by other associated fractures elsewhere in the assembly.

It is also of interest to note that the region of interest in confined on all sides by relatively rigid materials- the OD is jacketed by the threaded nut, the ID is buttressed by the copper tubing, and the end is being compressed by the ferrule. The material surrounding these cracks has relatively little room for large-displacement plastic deformation to occur. However, creep fracture of POM has been observed even when relatively little plastic deformation occurred- as little as 3% increase in overall length of the sample at 18MPa for material with a molecular weight of 41 kg/mol. (Christopher J.G. Plummer, 2000). This is much lower than the elongation at yield for the material in tensile testing shown in Table 2.

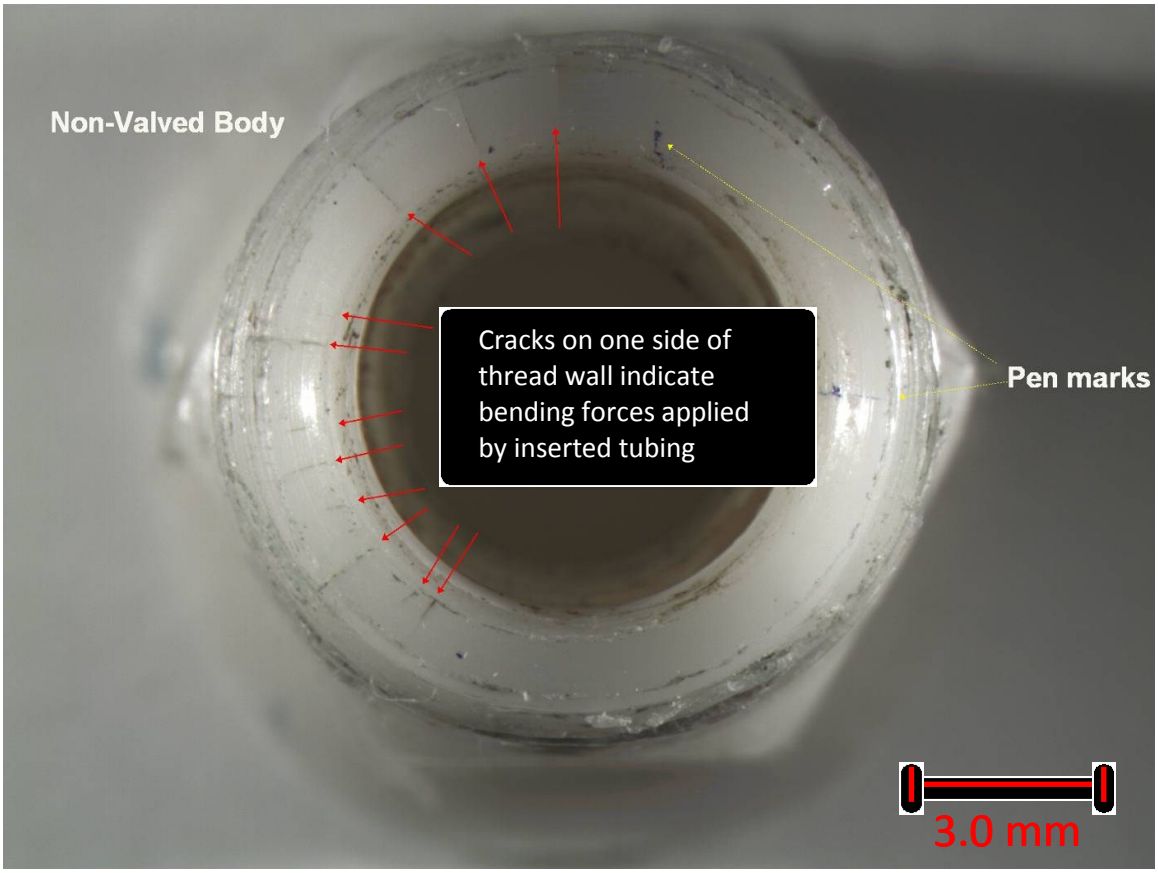

Figure 20: Optical micrograph showing cracks in the thread wall of a non-valved APC product used in the water filter application. Cracking along one half of the circumference indicates bending loads were applied to the tubing and transferred to the coupling. Had over tightening caused these cracks, they would be expected to occur around the whole circumference.

Bending moments are considered by Colder to be outside the design scope of the majority of its products- no ratings for bending have ever been formulated or determined to be necessary as couplings are not intended to bear mechanical loads.

The effect of pressure has been accounted for in the design of the coupling, and a specific rating has been offered by Colder. However, because Colder's products are generally designed for use with flexible plastic tubing, semi-rigid, bendable copper

tubing of the type used in residential plumbing may contribute additional stresses that would stack with normal (that is, accounted for) operating stresses.

Photos of filters as-installed are occasionally sent to Colder along with claim packets, and in some cases these images indicate that significant possibility exists for tubing-imparted stresses or other unanticipated applications. For example, consider Figure 21, Figure 22, and Figure 23.

Figure 21: Photograph of a return where the filter was plumbed with copper tubing and was unsupported. As the tubing stiffens over time due to cold work the bending forces produced will continue to increase.

Figure 21 is a typical installation with copper tubing. Note the copper inlet tubing leading to the filter on the left side of the image. As the refrigerator is pushed back into its position against the wall, that piece of tubing must bend to accommodate it. The tubing will act as a leaf spring and apply a bending moment against the filter if the filter

is positioned to resist that deformation. The stiffer the tubing and the more it is bent, the greater the bending moment and stress level on the plastic.

Figure 22: Photo of a filter installation where braided tubing was used and the filter appears to be unsupported.

Figure 22 is an unusual installation. It involves braided tubing, which is generally used on sinks and washing machines, but is not included in the water filter manufacturer's instructions for installation. Indeed, this kind of tubing is often not even compatible with a compression fitting, which means some modifications or adapaters may have been used in the installation. The nature and delicacy of those modifications is unfortunately unknown, and may have played a role in this failure.

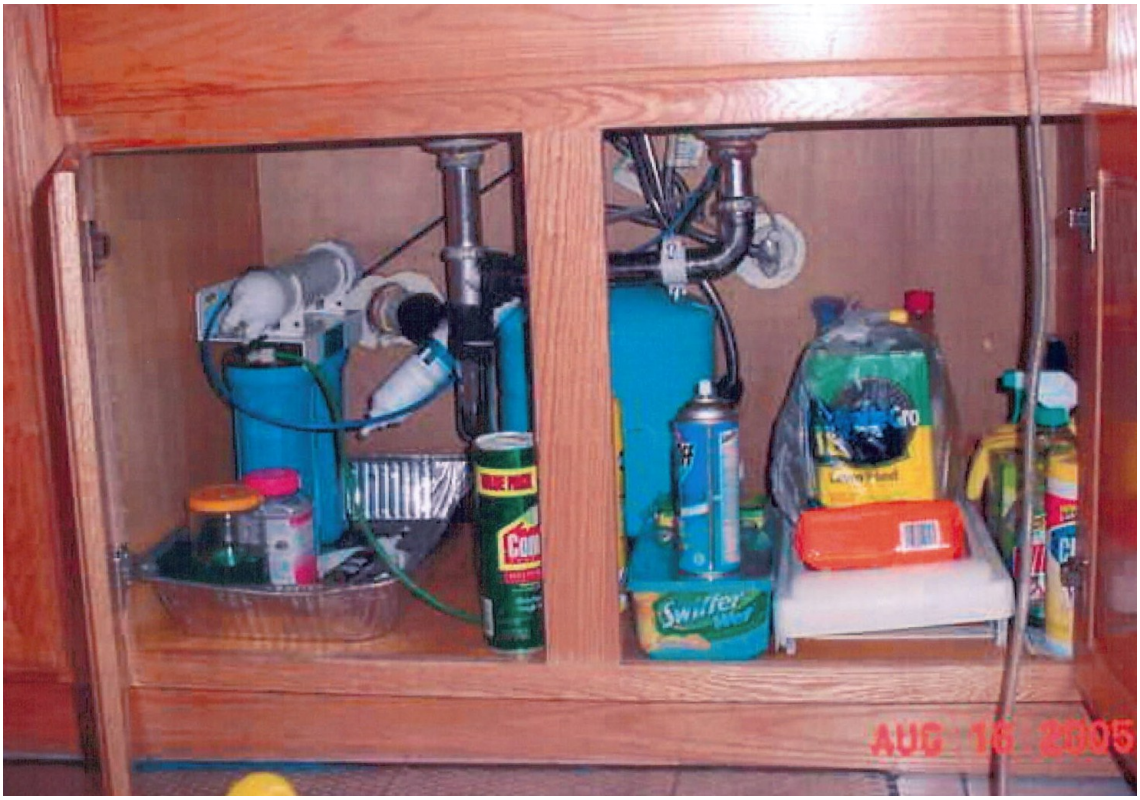

Figure 23: Photo of a filter installation under a sink. The kind of tubing used is unknown, but this filter was plumbed with hot rather than cold water, and was an inlet filter to an "instant" water heater.

Figure 23 shows an installation under a sink. This is not an installation method identified in the filter's installation instructions. Indeed, much about this installation was improper. The filter was plumbed in line not with a refrigerator, as designed, but in line with an instant on water heater for a kitchen sink. The filter was plumbed with hot water, not cold water as the filter manufacturer intended. In addition, it is installed in a location even more cramped and inaccessible than behind a refrigerator. Filter changes could require even more movement and deformation of the tubing, leading it to become harder and stiffer after fewer changes. This would lead to greater bending forces.

In order to attempt to quantify the level of bending moment that might be imparted by tubing, an apparatus was constructed to facilitate torque measurements. While more sophisticated measurements are surely possible, part of engineering is improvisational. A torque wrench was fixtured to a flat surface, and to the wrench was fitted a variety of copper tubing assemblies.

These assemblies consisted of a 12" length of ¼" OD flexible copper tubing installed to one port of a brass compression fitting elbow. The opposite port was fitted into a socket installed on the torque wrench. The copper tubing was then bent between positions consistent with a filter being pinned between two flat surfaces, such as between a rear grill on a refrigerator and a wall, and a position which may be achieved when a refrigerator is pulled away from the wall to allow access.

For each cycle, the torque registered at the wrench for the outward and inward strokes were recorded. A total of 19 cycles (outward and inward strokes) were performed. Three different copper samples were tested in this manner. Two were from a commercial product purchased new, similar to what new installers would have available from conventional sources. One sample was from an industrial supply house which was noticeably harder and stiffer, though whether such differences are due to alloy composition or cold work history is unknown. While such considerations may seem

important from a scientific point of view, it is worthwhile to realize that the material selected for use with the filter assembly in the field is outside of Colder's control all together, as is the method of installation. Therefore, striving to achieve greater levels of precision in material specification in experiment than is possible in the field is fruitless.

Instead, the goal of this experiment was to determine an approximate rage of torques which may be encountered in the application. The results of the experiment are shown below in Figure 24.

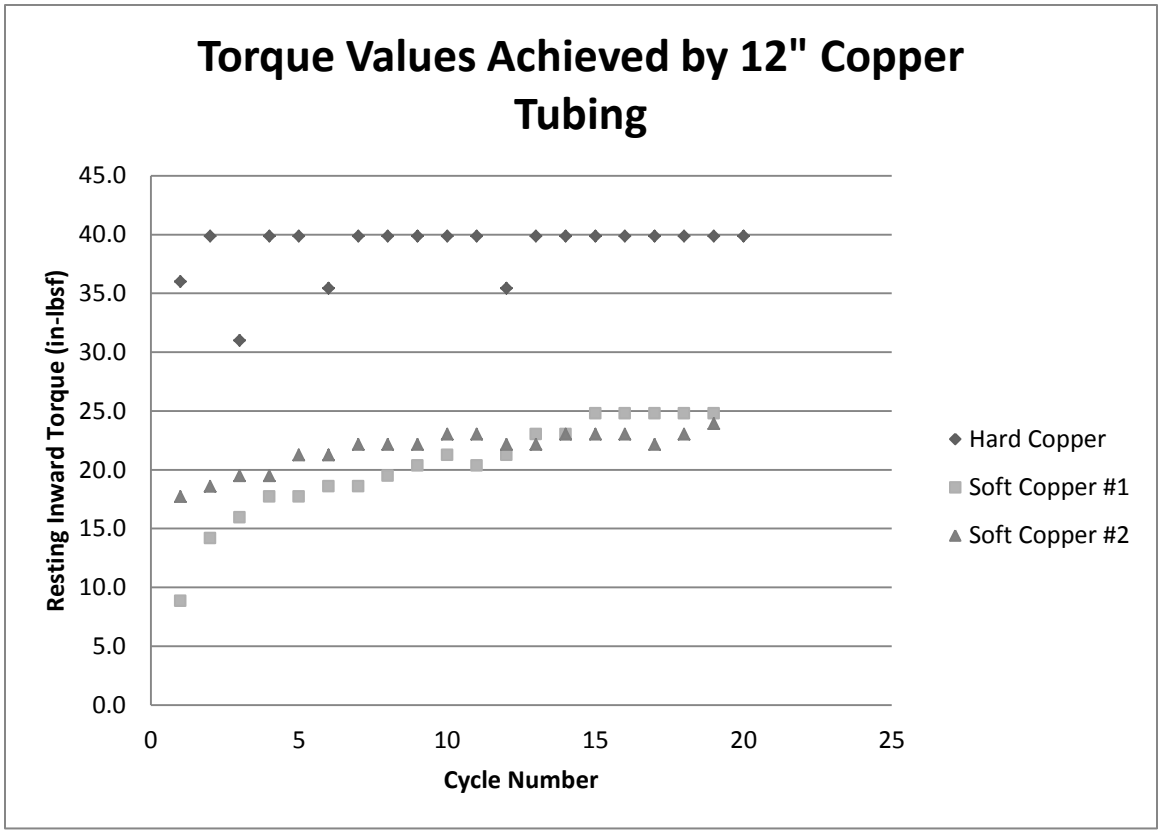

Figure 24: Plot showing torques achieved by bending lengths of copper tubing to approximate effects of filter replacement.

The experimental apparatus is shown below in Figure 25. In that figure, the two pieces of soft copper are shown after their cycle tests have been completed. Note the different shapes of each of the samples. The lower sample, with the more pronounced curve, was soft sample #1. The upper sample still fixture in the apparatus is soft sample #2. This is likely due to slight differences in the way the sample was bent back against the hard stop in each cycle, compounded over time, which led to work hardening in different areas of the material. Again, this variability is of concern from an absolute point of view, but considering the application, when no controls whatever are imposed upon the way the tubing is bent, it is apparent that these conditions are in our favor in that they demonstrate a degree of stability. The two sets of measurements for these pieces are rather close to one another, which indicates insensitivity to the specifics of the bending conditions. For our purposes of defining typical achievable torques, these data are adequate.

After cycling the hard sample over the same stroke as the soft samples, the part was reversed in the fixture to bring the opposite end of the tubing into the fixture. This allowed the same part to be used twice, given that additional samples of this material were not available for evaluation. The opposite end of the sample was similarly cycled, except across a greater travel, bringing it repeatedly to the point of kinking. This was believed to allow determination of the maximum achievable amount of torque the tubing would withstand before gross plastic deformation would limit the transference of

additional force. In this experiment, the maximum achieved level of torque remained 40 in-lbs, indicating that for the harder of the two tubing types available, 40 in-lbs appeared to be the maximum load that a part could be expected to see in service.

Given that bending moment of ~180 in-lbs will break a connector at the threads, 40 in-lbs is not a force to be dismissed, either in terms of a cause of creep loading, or in terms of establishing a baseline level of stress upon which fatigue loads from pressure or other forces would stack.

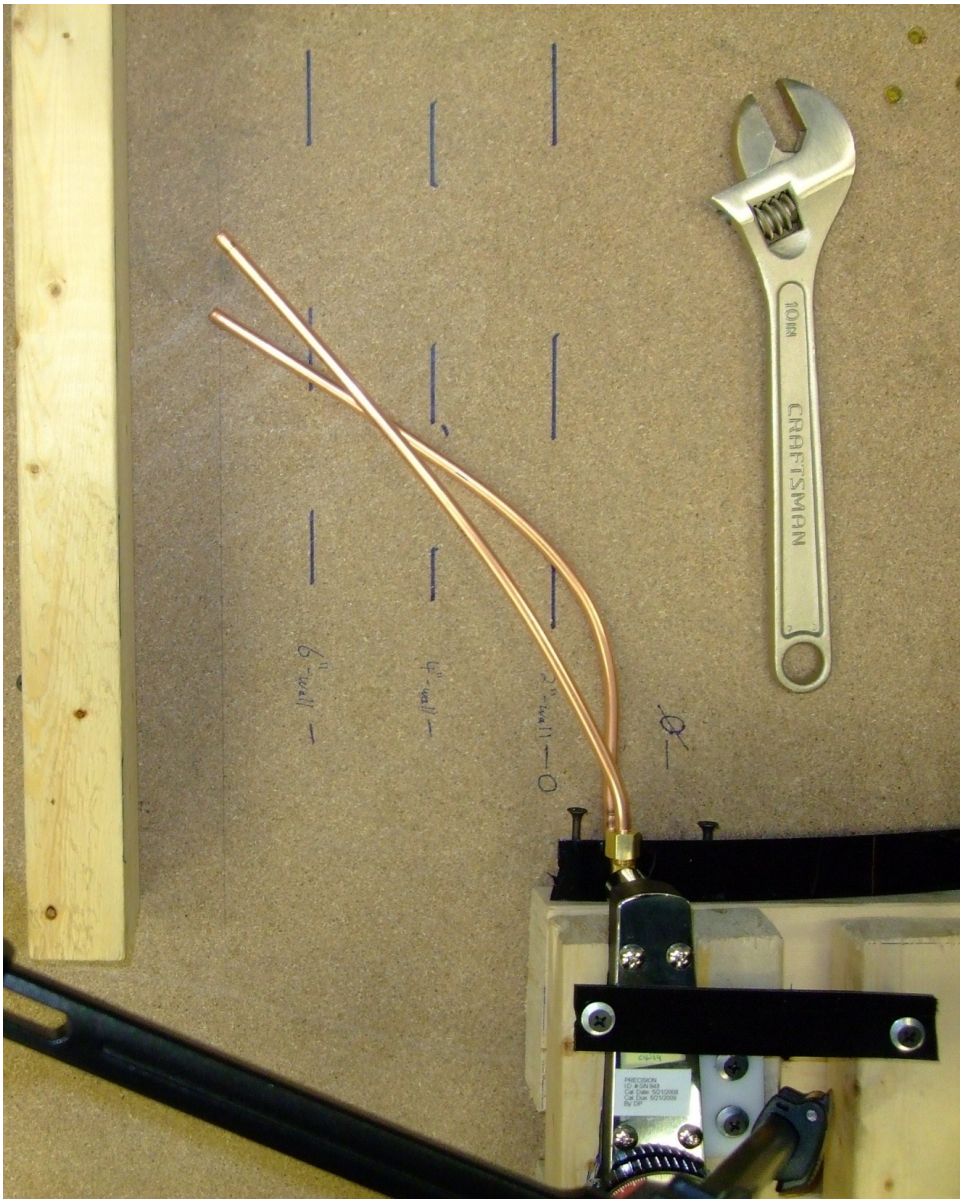

Figure 25: Photograph showing torque measurement apparatus. The torque wrench is fixed, and the tubing is bent back and forth against the movable hard stop. In this case, the stop is in the outward stroke position.

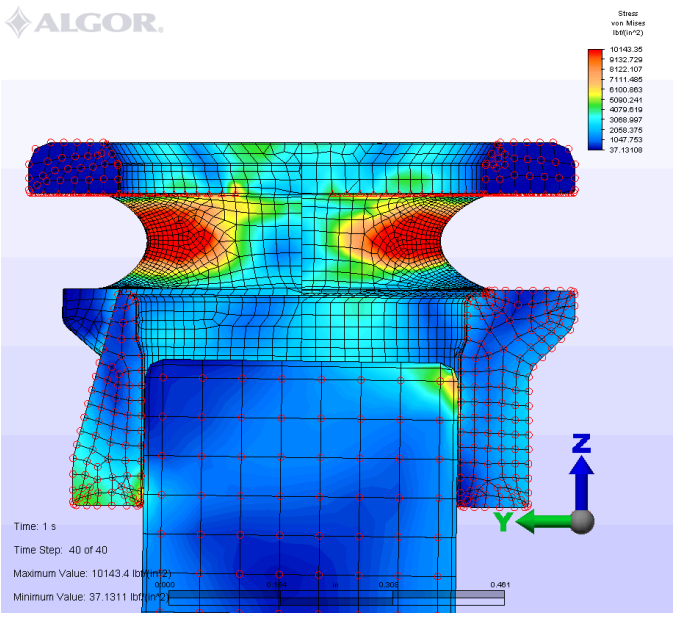

Figure 27: FEA Simulation of effect of interior bending force of 8.5 in-lbs (.95 Nm).

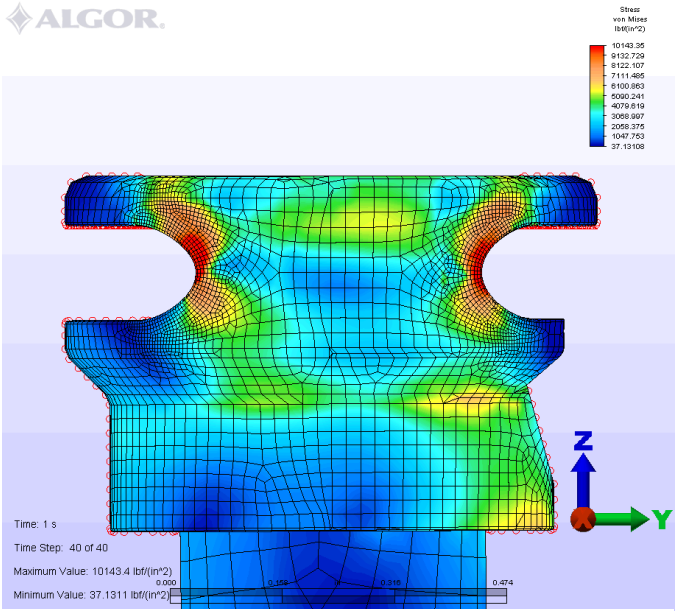

Figure 26: FEA Simulation of effect of interior bending force of 8.5 in-lbs (.95 Nm).

In order to determine the level of stress that such a bending moment may generate in the clip groove region, a Finite Element Analysis (FEA) was conducted using Algor. In this analysis, a rigid beam was modeled inside the inner bore of the part used in the analyses above. This beam was simulated with a force applied to the free end, imparting a bending force on the connector. The surfaces normally in contact with the thumblatch were considered to be fixed. Two different torques were simulated. Both simulated torques were lower than the measured values.

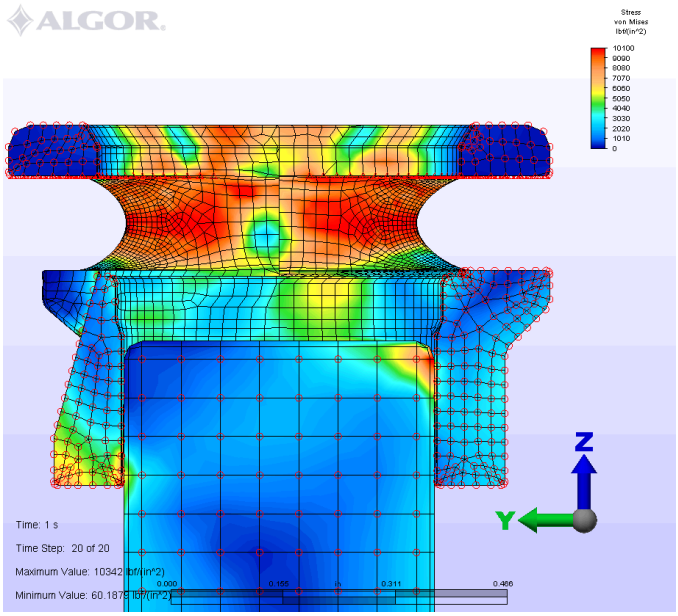

Figure 28: FEA Simulation of effect of interior bending force of 15.5 in-lbs (1.74 Nm).

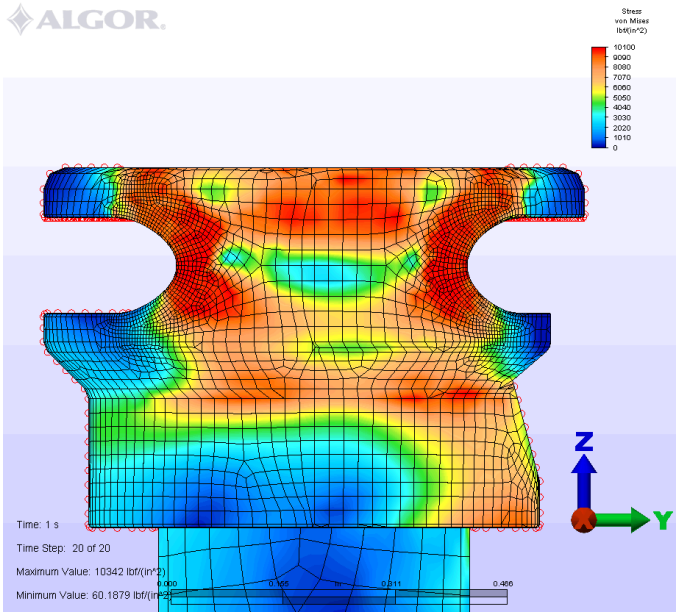

Figure 29: FEA Simulation of effect of interior bending force of 15.5 in-lbs (1.74 Nm).

The results of these simulations indicate an intense stress field arises from relatively small bending moments. Given that both sets of images are from analyses with stresses lower than that which even the softest tubing measured at the earlier points of its useful life could impart, it is clear that these loads are attainable. The stresses resulting from this loading are subject to the same kind of miscorrelation as was noted in the pressure section above. In order to check the magnitude of the bending stresses calculated by the software to experimental results, an APC body was connected to an insert and a rigid piece of tubing was inserted into the compression termination. This rigid tube was loaded at a distance of 12 inches from the compression

bore. A force of 15 lbs (180 in-lbs torque) broke the compression thread from the remainder of the body. This indicates that the simulation again fails to yield absolute values that correspond to experiment. This may be due to the stresses being born by different portions of the body that are more robust than the ears as well as the issues with load distribution in the program as noted in the tensile simulations.

Fractography:

Known Fatigue Samples

Many of the reports submitted to Colder claim to see evidence of fatigue in the fracture surfaces of returned parts. None of these reports, however, attempts to identify specific features as being hallmarks of fatigue- generally, a blanket statement is made that “striations” or “river markings” were observed on the fracture surface. The vagueness of these claims led to an effort to determine what a fatigued sample of this component would look like.

The POM material used to make APC series couplings is inherently extremely fatigue resistant owing to its robust crystalline structure and exceptionally high deflection at yield. Intentional fatigue of the APC, however, was found to be possible with the aid of Bill Mook and Megan Cordil, then PhD candidates in the Gerberich research group at the University of Minnesota.

By applying a linear force of 110 lbs (489 N) at a 1 Hz frequency to minimize the effect of heat buildup, it was possible to generate fatigue in an exemplar part after ~5565 cycles. This sample allows fractography of fatigue striations generated under a low-cycle regime. A fractograph captured with an optical microscope is shown Figure 30.

Figure 30: Optical micrograph of intentionally fatigued exemplar part.

Note that the striations are not continuous across the whole fracture plane. In this sample, the crack progressed incrementally across the crack length- creeping forward over a portion of the overall length at a time. Each location of advance formed a striation. As such, the striations are small and quite localized and only a high resolution microscope is able to resolve them.

A sample was also fatigued in the high-cycle regime. This was accomplished more "realistically" than through the use of a load frame, where time availability would make a test of this duration at appropriate frequencies impractical. Instead, parts were fixtured in Colder's cycle test equipment. Inserts and bodies were sealed and pressurized to 120 PSI. Then, each assembly was subjected to mechanical tension through the use of air cylinders operated by PLCs. Tension of ~70 lbsf was applied at

frequency of 1Hz. This more accurately simulates the effect of water hammer in that the parts were under steady load from pressure at all times, with momentary spikes in stress. This loading required over 150,000 cycles to initiate cracks.

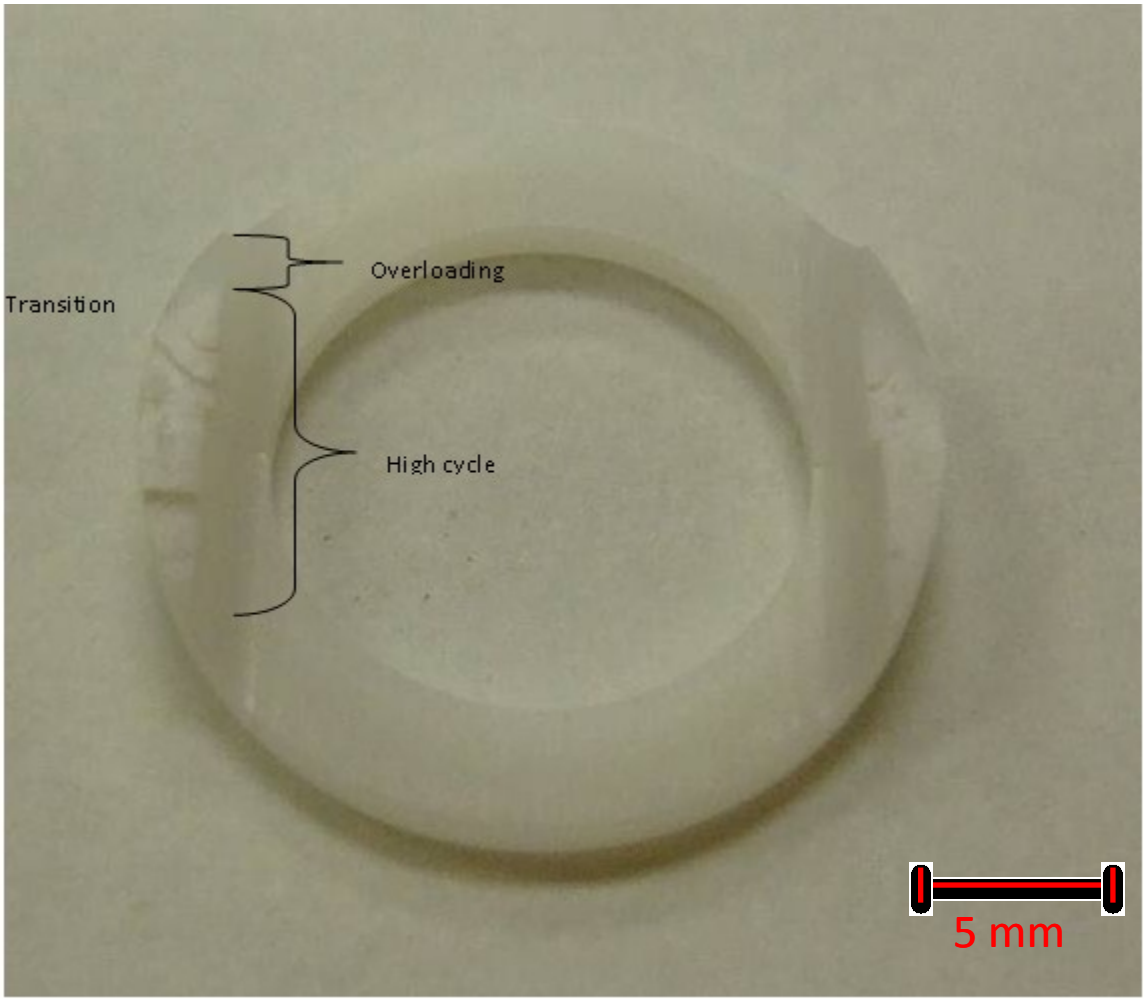

Figure 31: Photograph showing the fatigue and overload portions of the fracture surface of a known high cycle fatigued component.

A view of a part that was mechanically fatigued in the laboratory through over 200,000 cycles is shown in Figure 31. Note the characteristic chalky white appearance of the fatigued region, which transitions to the more natural color in the simple fracture region. This color difference is not seen in the fractured valved body.

In addition to the texture in such a high-cycle fatigue sample, there appears to be a transition region where the fracture progresses from a high cycle propagation mode to an overloading mode, and in that transition region the crack moves in a low-cycle

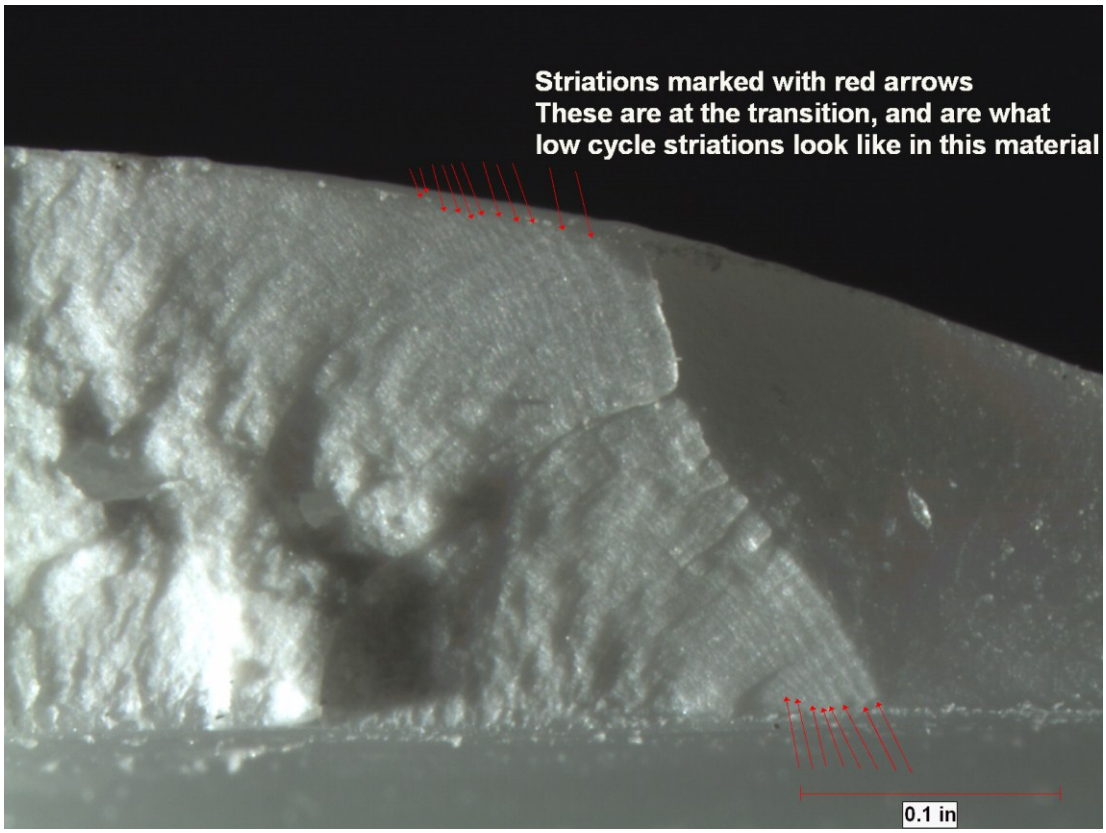

Figure 32: Optical micrograph of the transition region of the sample shown in Figure 31. Red arrows indicate the location of striations showing crack arrest during the transition from fatigue into overloading.

fatigue regime that is easier to detect. Figure 32 shows the striations in such a region of the sample. This same part was further analyzed using electron microscopic techniques to evaluate the surface morphology in the initiation, transition, and final failure areas of

the fracture surface. Local evidence of fatigue striations was found over a portion of the fracture surface, identified in Figure 33.

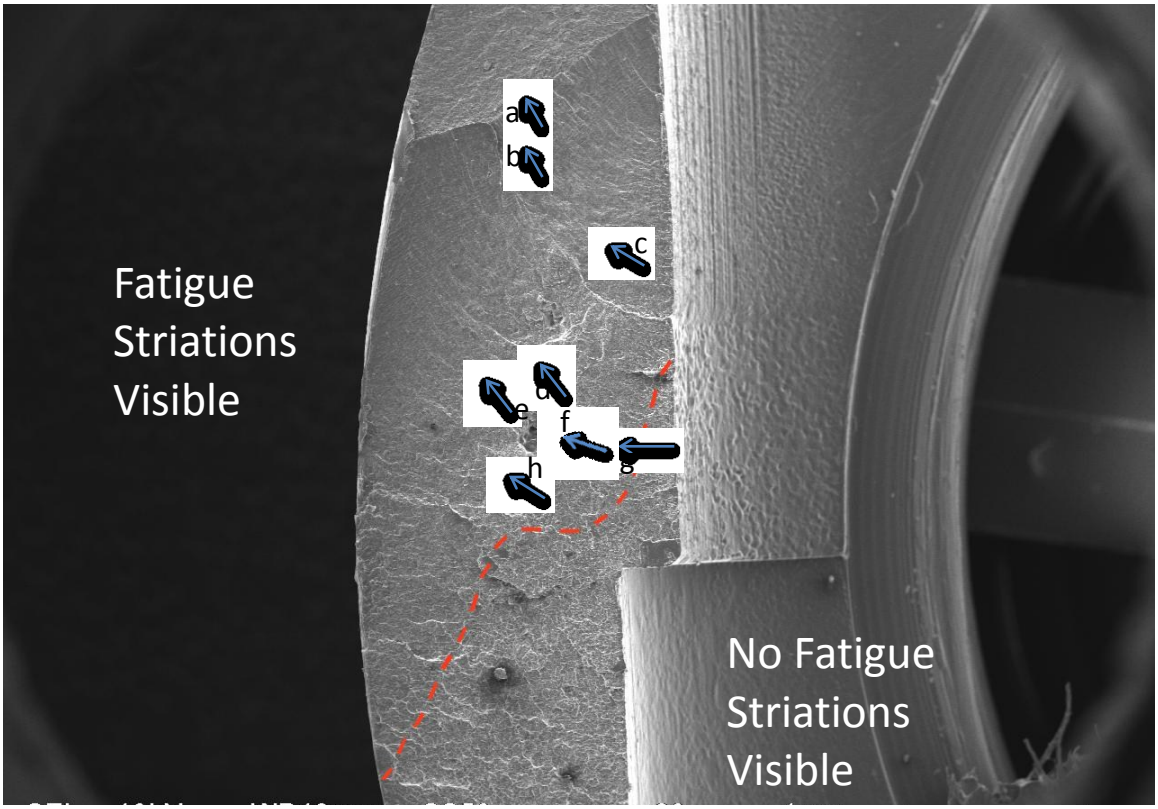

Figure 33: SEM image of high cycle fatigue sample. Above the red line, evidence of striations was visible. Below the line, striations were not found. Letter references indicate relative positions of subsequent SEM image captures referenced below. Arrows show direction of crack progression in each image.

These two examples, showing both small scale, local evidence of fatigue (in the low cycle regime) and larger striations across the whole sample (in the case of the transition region in high-cycle fatigue) characterize the full scope of observed fatigue.

The high cycle specimen shown in Figure 31 was further analyzed to determine:

1.) The crack progression as a function of stress intensity.

2.) Whether the point of final failure coincided with the critical stress intensity factor for the Delrin raw material.

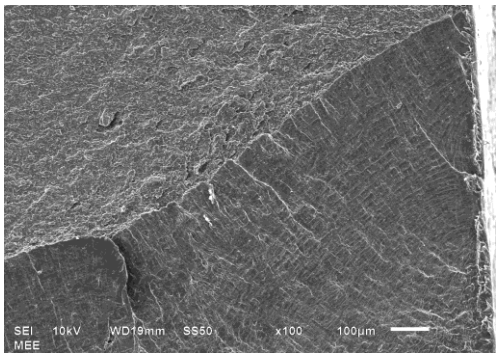

a

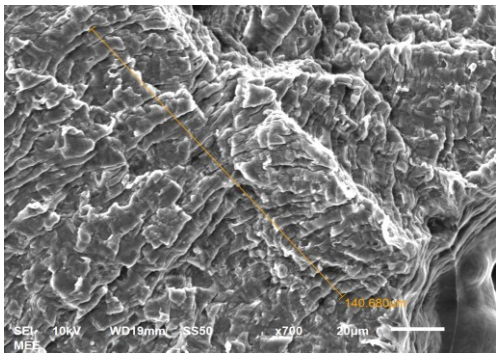

e

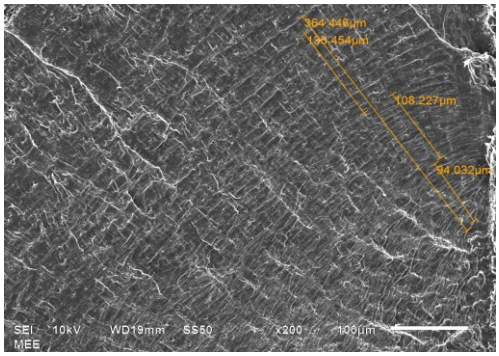

b

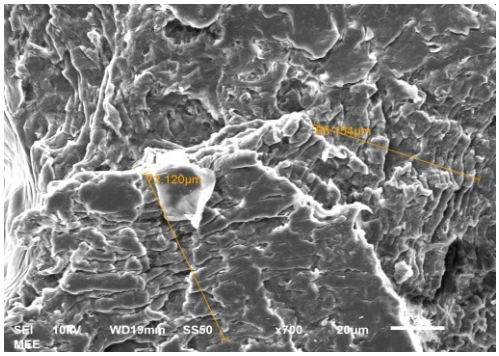

f

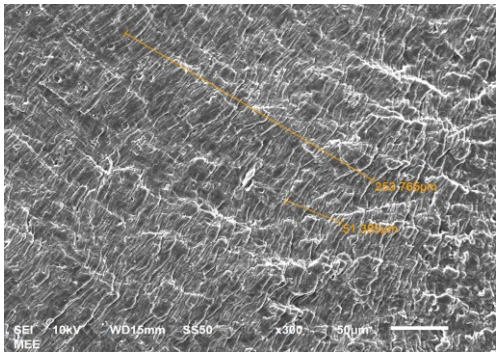

c

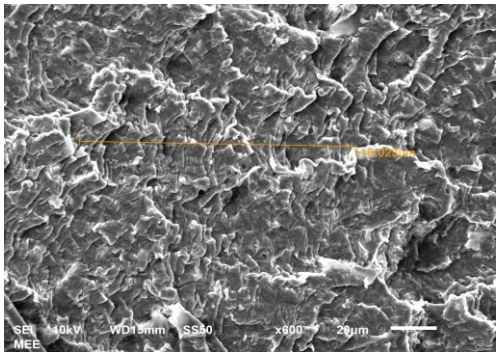

g

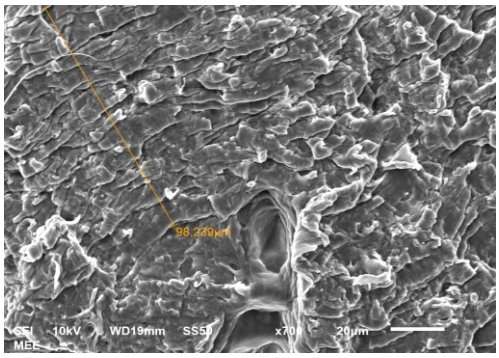

d

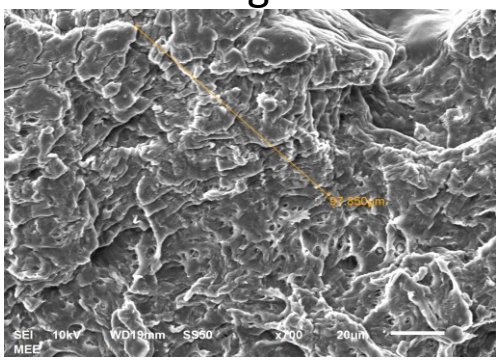

h

Figure 34: SEM images used for crack progression analysis.

Each of the images shown in Figure 34 provided one or more data points for this analysis. The location of each image on the sample was determined using the coordinates captured in the SEM data files.

The sample cross section was approximated as a rectangle. The crack length at the transition to simple fracture was determined by measurement of the location of the center of the transition line to the far edge of the sample. This length was measured to be .0066m, compared to an overall sectional length of 0.0118m.

Each crack growth rate data point was generated by counting fatigue striations intersecting measured distance lines draw perpendicular to the direction of crack advance. The overall crack lengths at each data point were determined based on the coordinates of the SEM stage when the image was taken compared to the coordinates of the stage at the point of transition from fatigue to fast fracture.

Table 4: Striation spacing data versus change in stress intensity.

Image Name	a (m)	Count of striations	Line length (microns)	Line length (m)	da/dn (m/cycle)	Delta K
a	0.0066	9	141.0	1.41E-04	1.6E-05	1.74
a	0.0066	5	141.0	1.41E-04	2.8E-05	1.74
b	0.0066	8	133.5	1.33E-04	1.7E-05	1.76
b	0.0065	19	108.2	1.08E-04	5.7E-06	1.73
b	0.0064	18	94.0	9.40E-05	5.2E-06	1.68
c	0.0059	12	51.4	5.14E-05	4.3E-06	1.37
c	0.0059	54	253.7	2.54E-04	4.7E-06	1.37
d	0.0049	38	98.2	9.82E-05	2.6E-06	0.97
e	0.0047	51	140.7	1.41E-04	2.8E-06	0.90
f	0.0046	23	72.1	7.21E-05	3.1E-06	1.04
f	0.0046	16	65.2	6.52E-05	4.1E-06	1.04
g	0.0044	40	118.0	1.18E-04	3.0E-06	0.83
h	0.0044	35	97.9	9.79E-05	2.8E-06	0.85

The stress intensity values were determined based on the loads applied to the part during the fatigue process. At the maximum condition of the cycle, approximately 124 N were applied to the specimen. At the minimum, 32 N were applied. Stress intensity was calculated based on the equation (Hertzberg, 1996).

$$K_1 = Y \frac{P\, a^{1/2}}{t\, W}$$

Equation 2

where K_1= is the stress intensity,

Y is a geometric factor based on a and w, and was determined from Hertzberg plot 8-7f for each a/w ratio

P is the load applied

a is the crack length

t is the thickness of the cross section (.00220m for this sample)

W is the width of the sample (.0118m for this sample)

Stress intensity was calculated for each crack length for the maximum and minimum loads. The difference between these stress intensities is reported in Table 4.

These results are plotted below in Figure 35 and Figure 39.

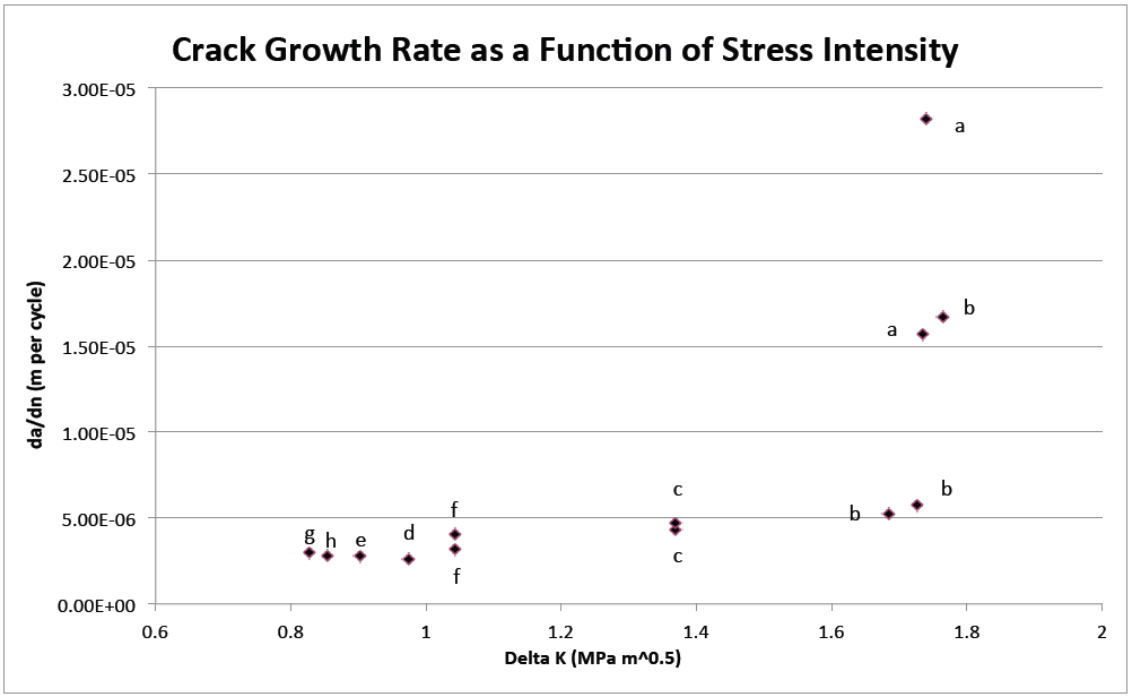

Figure 35: Graph showing experimental crack growth rates versus calculated changes in stress intensity values from high to low loads during the fatigue loading process. Each data point is tagged with the letter corresponding to the image it was derived from.

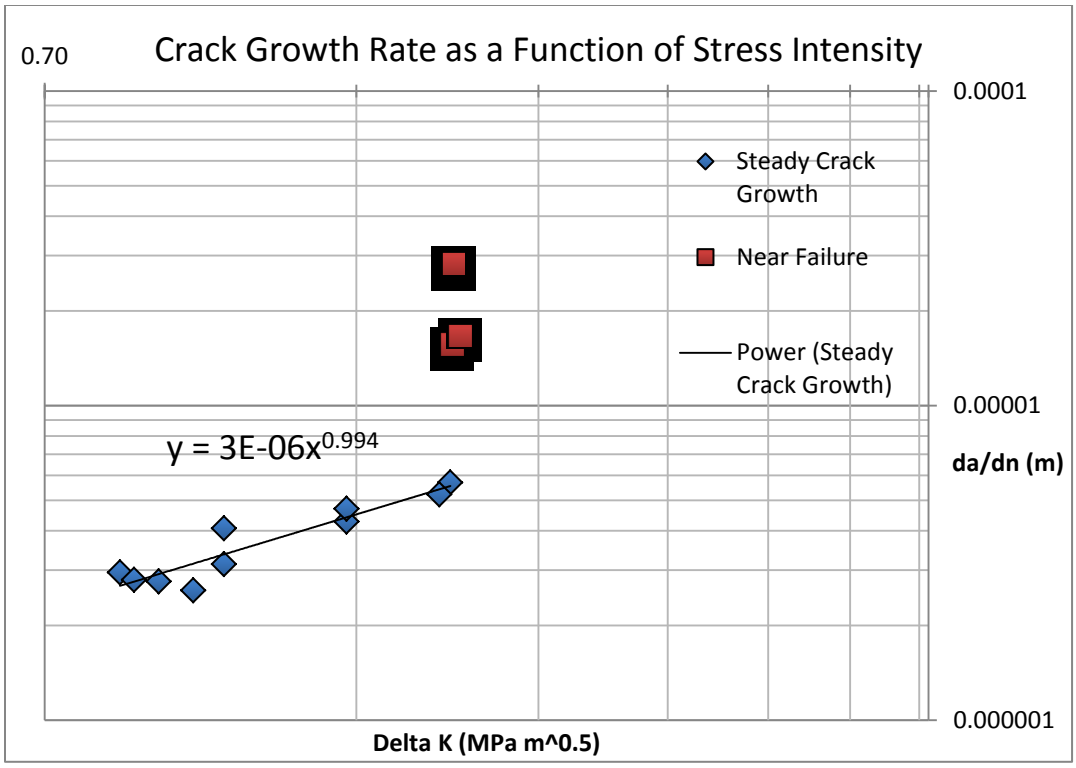

Figure 36: Graph showing the same experimental data shown in Figure 35 but plotted on a log-log scale. A clear shift in propagation behavior is seen between steady growth and propagation to failure.

Data points from images d, e, f, and h may be impacted by the presence of the void. However, despite the void being positioned between each of these images, the crack growth rates do not appear to have been significantly elevated compared to the rates seen for points from images g and c, which indicates that the void apparently had a relatively minor (and per this data, undetectable) impact on the crack growth rate. Examining the morphology of the fracture surface near the void indicates that the void was not the crack origin as the direction of crack advance is consistently toward the upper left in images all around the void.

As the crack advanced, it appears that it originated on the inner edge (right side of the fractured surface) and progressed leftward and upward as a increased.

The plot shown in Figure 35 is consistent with expectations, showing a long period of relatively constant crack growth across a wide band of ΔK values, followed by a sudden and sharp increase in growth rate. Some irregularity is evident in the points from images a and b immediately preceding final fracture. In part, this is due to the difficulty of establishing an accurate "a" length due to the crack progressing at an angle relative to the edges of the cross section and the larger crack length compared to the remaining unfractured length, W-a.

Evaluating the transition point from fatigue crack growth to simple overload fracture required a shift from evaluating ΔK to K_{MAX}. K_{MAX} is a function of the length of the crack, a, growing larger as the crack advances until the point of final fracture when K_{MAX} reaches the critical stress intensity of the material. The K_{MAX} at crack length $a_{critical}$ is therefore the experimental K_{1C}, critical stress intensity factor.

Using Equation 2 at the crack length at the transition, a=.066m:

$$K_1 = Y\frac{P\ a^{1/2}}{t\ W}$$

$$K_{MAX} = K_{1C} = 6\frac{124N\ (.066m)^{1/2}}{.00219m\ .0118m}$$

$$K_{1C} = 6\frac{124N\ *.0812m^{1/2}}{.0000258m^2} = 2.34 \times 1010^6\ {}^{N}/_{m^{1.5}} = 2.34MPa * m^{1/2}$$

The experimental K_{1C} is thus determined to be 2.34 MPa*$m^{1/2}$. This compares favorably with Dupont's stated critical stress intensity of 2.4 MPa*$m^{1/2}$. (Dupont Engineering Polymers, 2006).

The calculation based on an idealized rectangular cross section agrees very closely to the experimental reality. The point of final failure was almost exactly identical to the one predicted, indicating that the actual cross section of the material which contains two relatively sharp corners and a corner notch in the middle of the interior wall did not appreciably affect the propensity of the part to fracture by fatigue. The formula used in the calculation above is intended to apply to rectangular sections of material. The actual section functioned experimentally like a rectangle.

Plotting the data on a log-log axis in Figure 36 allows the determination of the Paris law exponent for the equation:

$$\frac{da}{dn} = \alpha \left(\frac{(\Delta K - \Delta K_{th})}{(K_{IC} - K_{max})} \right)^{m}$$

where α = a constant

ΔK = the change in stress intensity from the minimum to maximum load conditions

ΔK_{th} = the threshold change in stress intensity required for a fatigue crack to advance in the material

K_{IC} = The critical stress intensity factor for the material

K_{MAX}= the maximum stress intensity at a given cycle

m = the Paris law exponent

From Figure 36 it is clear that the Paris law exponent for this system is approximately unity. The results obtained from this fatigued sample are similar to those reported for glass reinforced polypropylene (Alessandro Pegoretti, 1999). In these experiments on polypropylene, also a semi-crystalline polymer, the researchers found a similar Paris law exponent (~1 at low frequencies) and found that the exponent's value did not vary with glass fiber content at a variety of frequencies, including those samples tested at 1 Hz, the load frequency employed here for acetal.

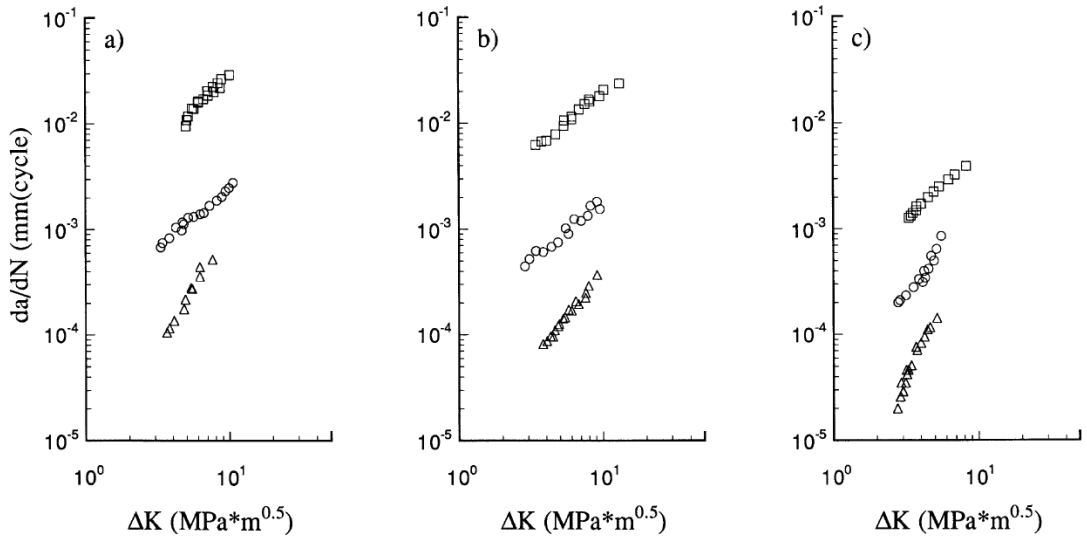

Figure 37: Paris plots of the stable crack growth regime for glass filled polypropylene. (Alessandro Pegoretti, 1999). Plot a) shows data from samples with 10 wt% E-glass reinforcing fibers, plot b) 20wt%, and plot c) 30%. □ data points were measured at .1Hz, O data points at 1Hz and Δ data points at 10 Hz.

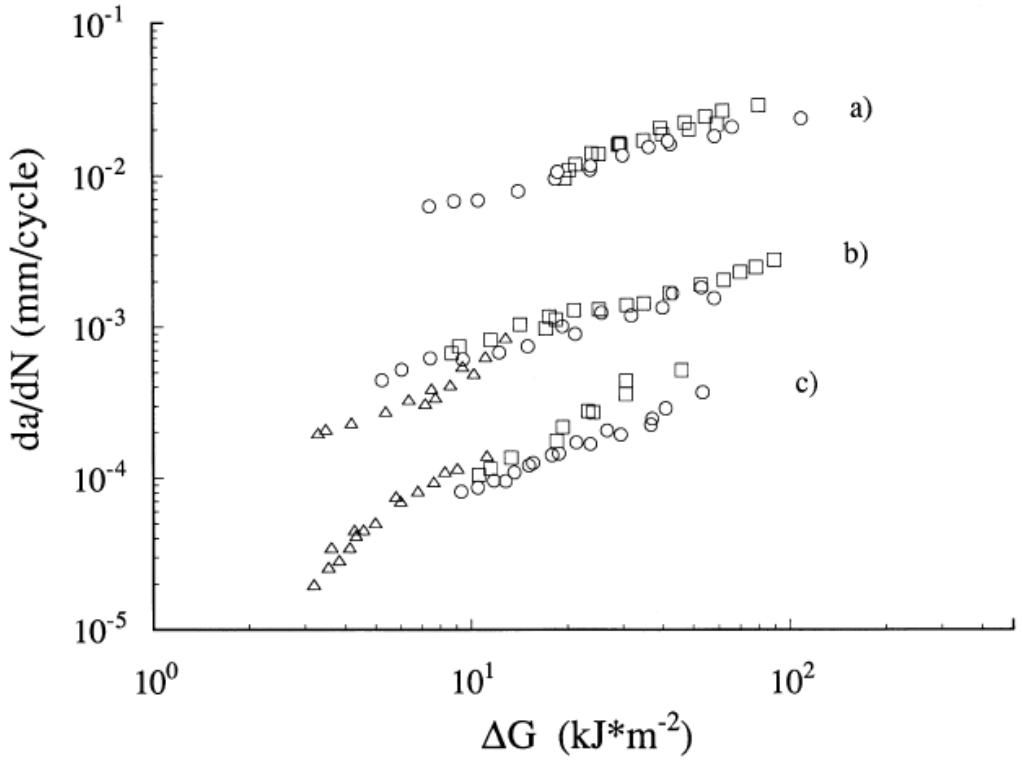

Figure 38: Plot showing the crack growth rate as a function of the strain energy release rate for various glass filled polypropylene samples. Data in set a) are from .1Hz, b) from 1 Hz and c) from 10 Hz frequencies. □ data points were from samples with 10 wt% glass, O data points were from samples with 20 wt% glass Δ data points were from samples with 30 wt% glass. (Alessandro Pegoretti, 1999)

Known Creep Sample

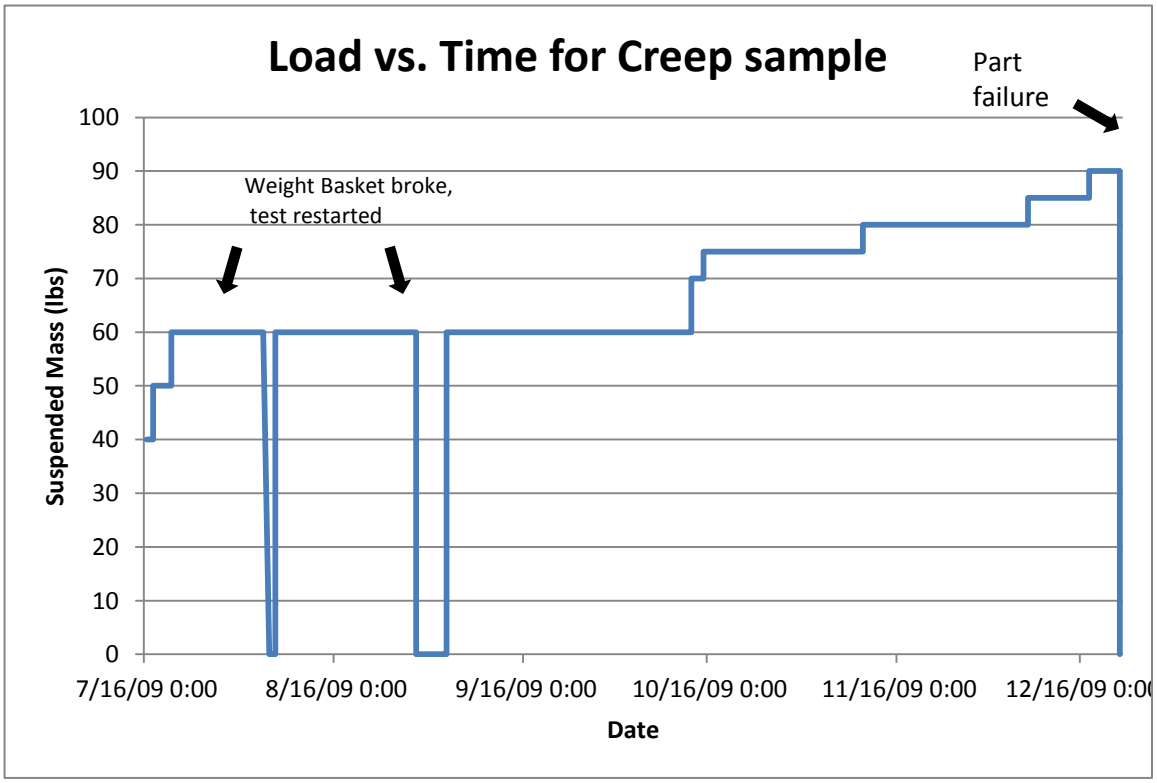

Figure 39: Plot showing the weight suspended from the creep sample in order to generate the failure. Twice the polypropylene basket used to hold the weight failed before the part did. When this occurred, the test was re-started after making repairs and modifications to the suspension system.

To facilitate a comparison of surface morphology between fatigued and creep ruptured samples, a specimen was intentionally exposed to long term, high levels of load. The load was imparted by hanging weights from a coupled APC body/insert set. At several points during the experiment the load was carefully increased in order to generate fracture in an experimentally viable time period.

The resulting sample was evaluated using SEM techniques to capture images of the resulting fracture surface. Three different zones bearing different morphologies were observed:

1.) An initiation region, showing multiple planes with evidence of separation/crazing, with fibers bridging between two opposing surfaces.
2.) A fibrous region of high plasticity showing significant drawdown of fibers from spherulites.
3.) A region of fast fracture, showing little evidence of plasticity (little drawdown) with a plate-like appearance to the fracture surface.

Figure 40 shows these three different zones in close proximity to the point of initiation. Figure 41 shows four images of the initiation zone on the opposite half of the same part as that shown in Figure 40. Note the similarities to the graphic in Figure 12, which shows the craze initiation process in a polymer thin film. Here as well it appears that multiple planes of local crazing coalesce to form a variety of craze planes, before one becomes dominant and fracture begins progressing more quickly due to the reduction in bridging molecules in that zone (Schultz J. , 1984).

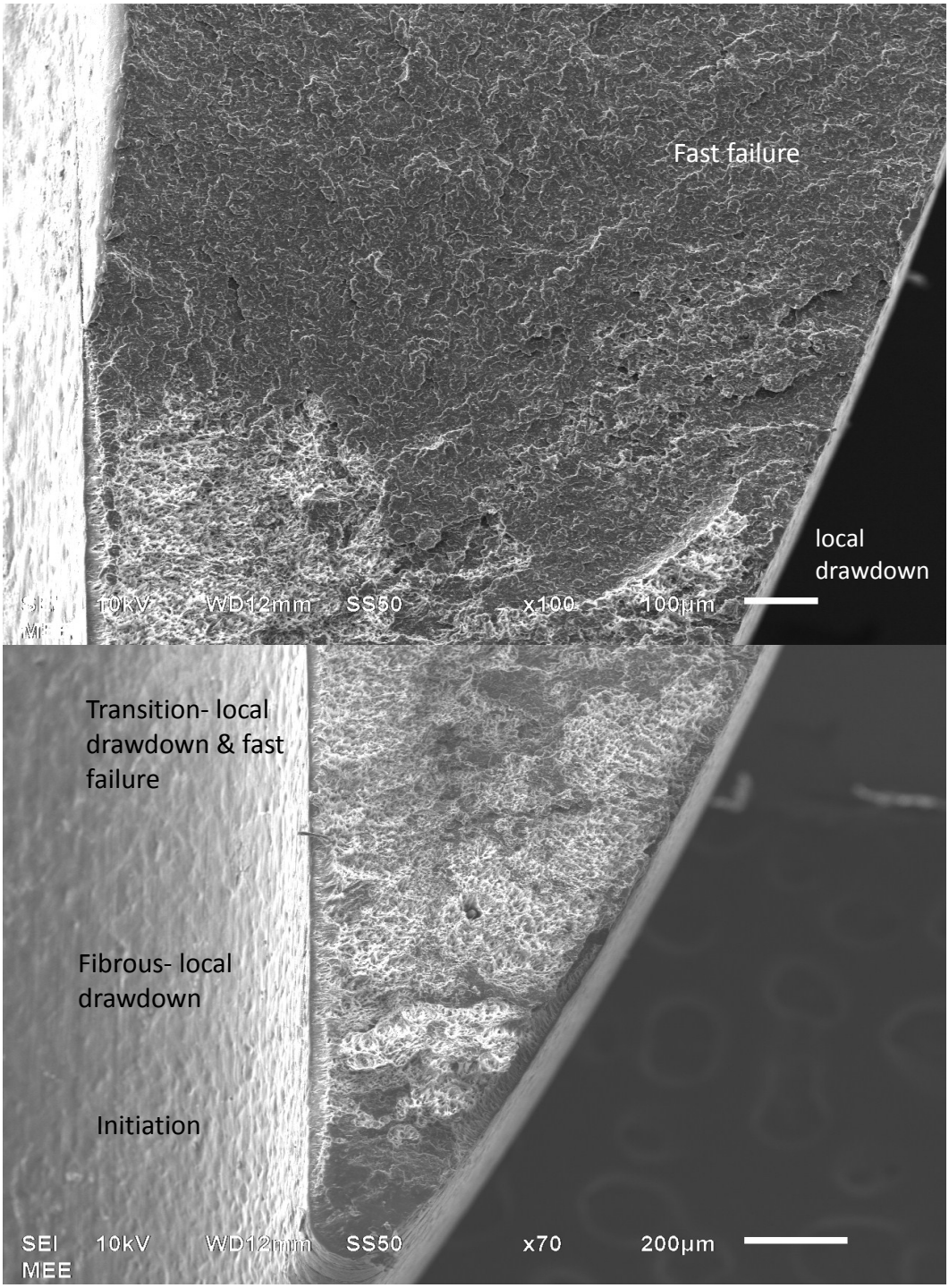

Figure 40: SEM images showing three different surface morphologies near the point of initiation. The two images shown are of adjacent portions of the same surface.

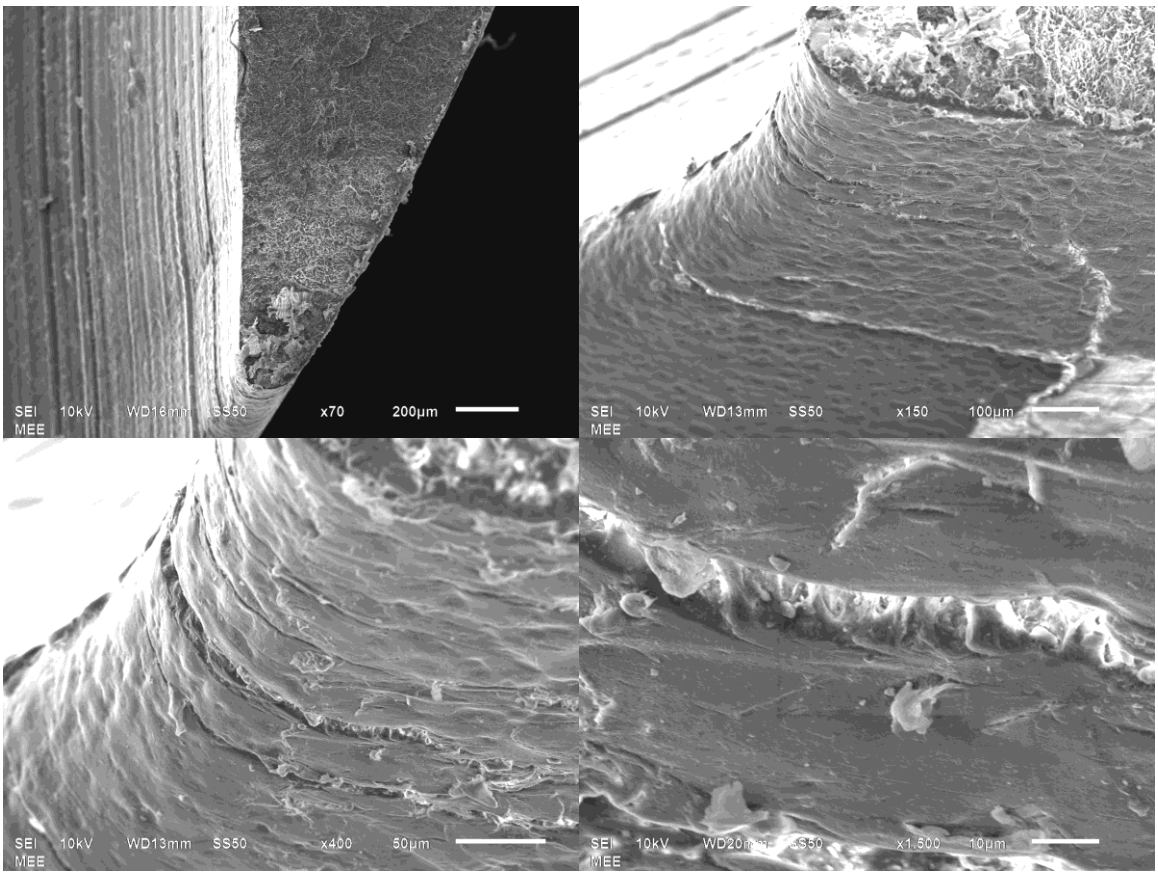

Figure 41: SEM micrographs showing the initiation region of the opposite half of the part shown in Figure 40. Top left: overview showing the same initiation, local drawdown, and fast fracture regions. Top right: oblique view of the edge of the part with the fracture still in view. Note points of separation under the fracture plane where additions fractures began to develop as crazes before the final fracture occurred. Bottom left: closer view of the crazes/secondary fractures. Bottom right: closer view of the crazes.

Fiber drawdown in this sample is particularly pronounced, as shown in Figure 42. This is consistent with the behavior observed when sufficient numbers of molecules bridge between spherulites to facilitate the shearing of polymer molecules within the spherulite into fibers to bridge the craze plane. Portions of the sample showed a wide ribbon of drawn down material.

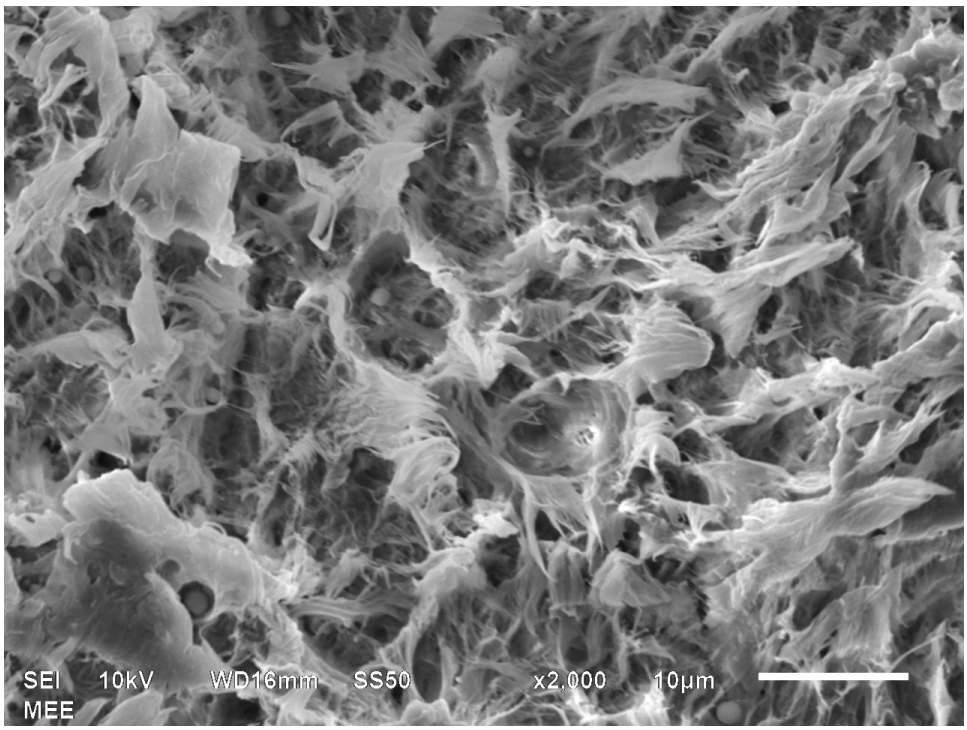

Figure 42: SEM showing local drawdown zone of creep sample.

The transition region shows both fiber drawdown and a new surface morphology that looks somewhat similar to the high cycle fatigue region shown in Figure 34. The key difference between this surface morphology and that of Figure 34 is the repetition of the orientation of the edges, which were consistent in the fatigue sample, showing parallel edges indicative of the advance of the crack front. In the creep sample the same edges are observed, but their orientation is not consistent across significant distances, though over shorter distances it can appear that parallel edges do exist.

The transition and fast fracture surface morphologies are shown in Figure 43 and Figure 44.

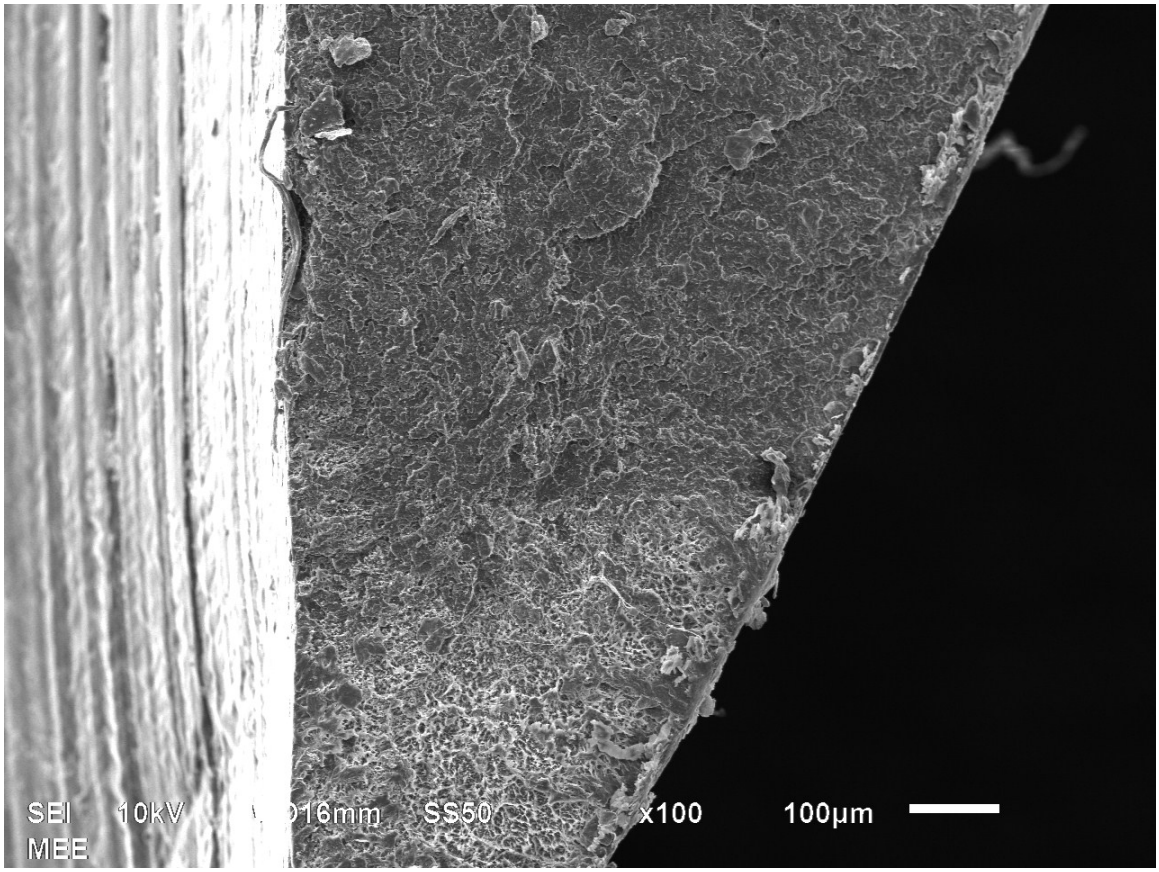

Figure 43: SEM of the transition region in the creep sample.

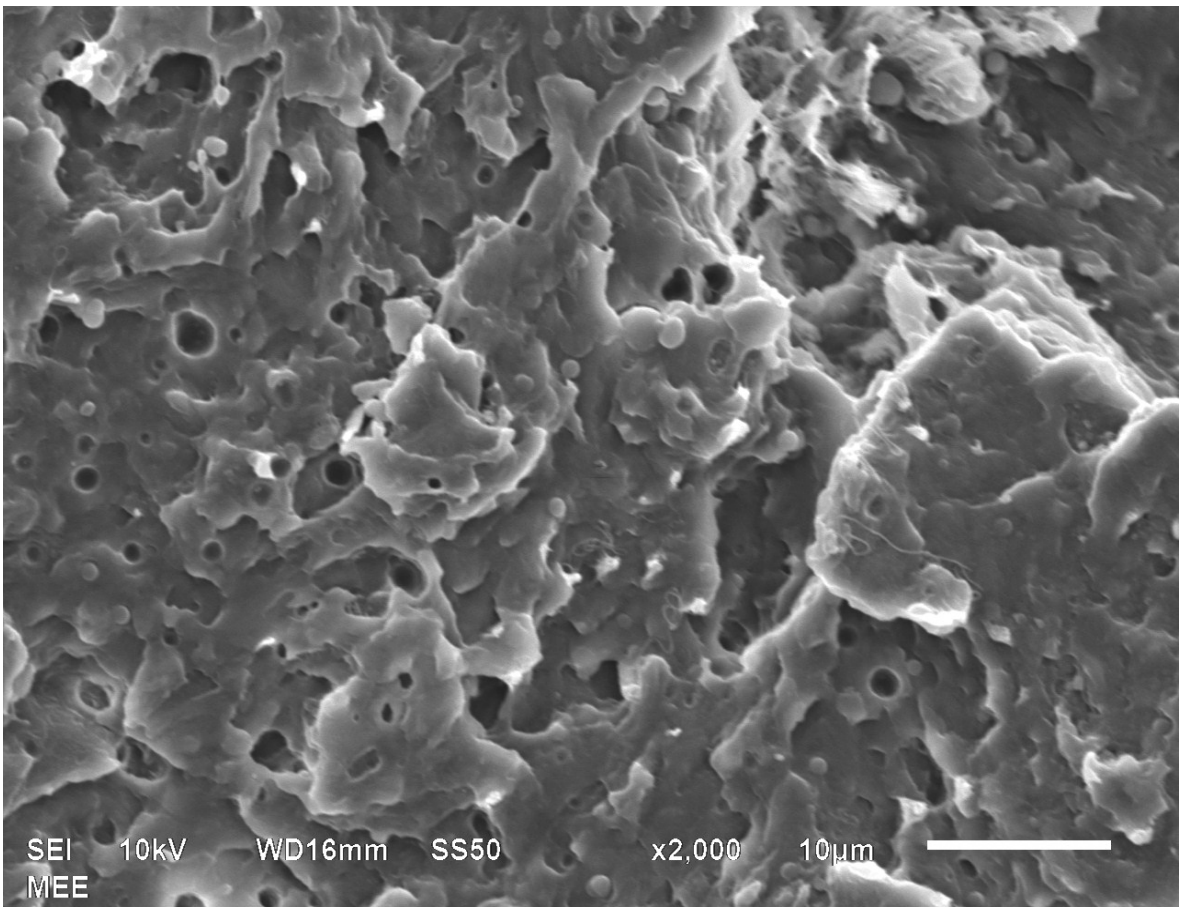

Figure 44: SEM of the fast fracture surface morphology in the creep sample.

Known overload sample:

Having identified characteristic features associated with both creep and fatigue loaded samples, a third sample was prepared an analyzed after intentionally applying a force ramping from 0 to 140 lbs-f sufficient to cause breakage within a few seconds of load application. This load was applied using a screw driven load frame, with a body held by the threads and the insert held in a collect. Rotating the drive screw moved the body away from the insert, and a load cell recorded the peak force achieved during the break.

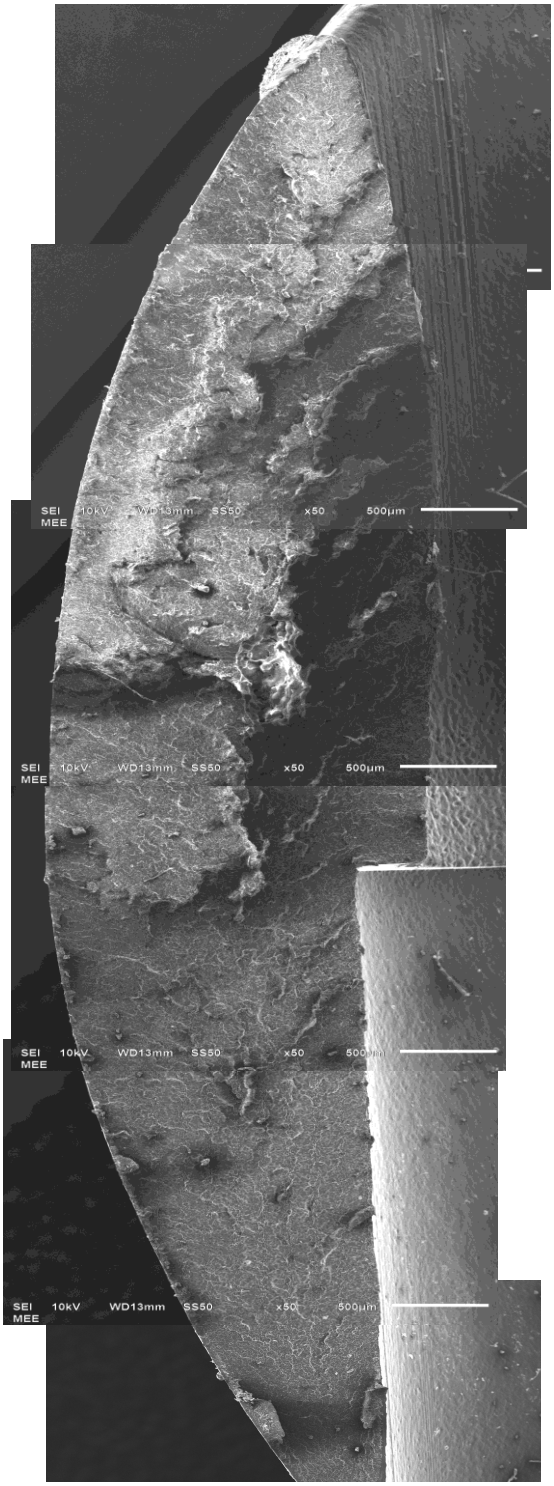

Figure 45: Knit images of the overload fracture sample showing the complete fracture surface.

This sample was then analyzed with a scanning electron microscope. As with the other samples a gold coating was applied to minimize charging artifacts.

Figure 45 shows an assemblage of 6 different SEM images, all captured with the same magnification, knit together to show the full fracture surface in one image. The fracture initiated at the bottom of the figure and progressed toward the top. Significant differences between this sample and the other two are evident.

1.) There is a brittle crack propagation zone at the initiation point (bottom)

2.) The fracture surface in the lower half of the fracture has fewer features than in the other two samples and generally shows less deformation/surface porosity.

3.) Significant plateaus are evident in the top half of the fracture surface, with significant "jumps" in the fracture plane

The initiation point indicated by the arrow in Figure 46 is relatively featureless and smooth and indicates the crack front formed via a brittle fracture mechanism- simple cleavage through the material where there was insufficient time for significant deformation of the spherulitic structure prior to failure. However, after a few hundred microns of crack growth the mechanism apparently changed and there is evidence of some microstructural changes in the material during the fracture process.

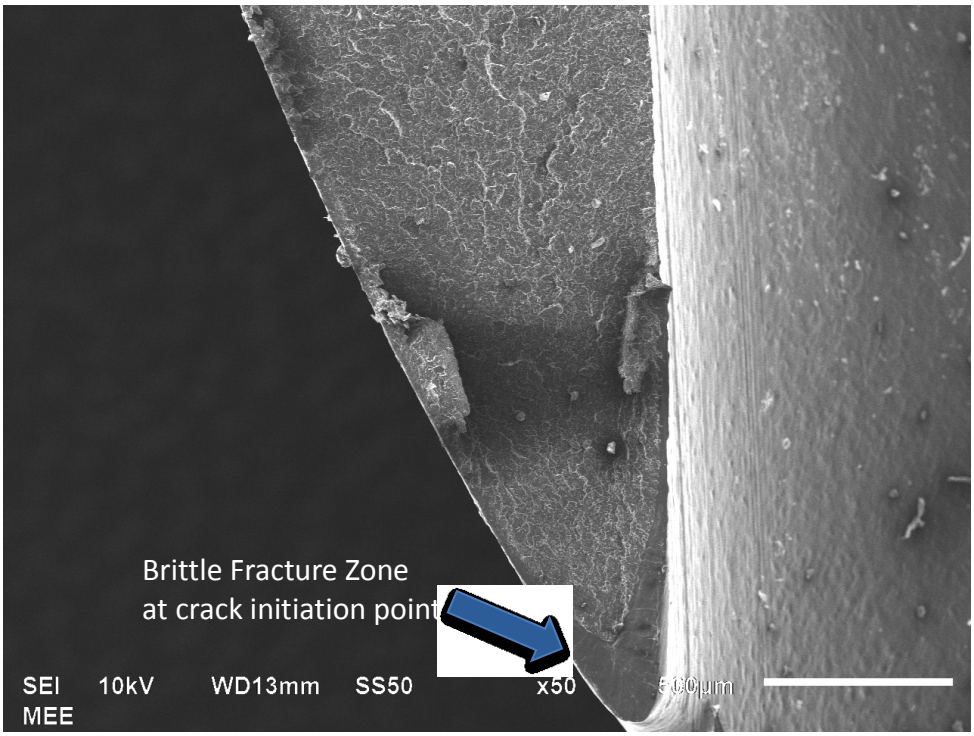

Figure 46: SEM image showing initiation region on an overload sample. Note the brittle crack region at the initiation point, displaying a smooth, featureless area. The crack growth mechanism in this region was apparently different than the mechanism which dominated the majority of the crack advance.

Evaluating the area of the fracture surface immediately above the initiation point reveals slightly more surface structure, but far less than was observed in the fatigue and

creep samples. Images from this region of each of the three samples are shown in Figure 47. The overload sample has similar surface features compared to the fatigue sample, but the fatigue sample shows more freestanding fibrils of material. The creep sample, similarly, shows even more surface fibrils caused by even more drawdown prior to separation of the fracture surfaces.

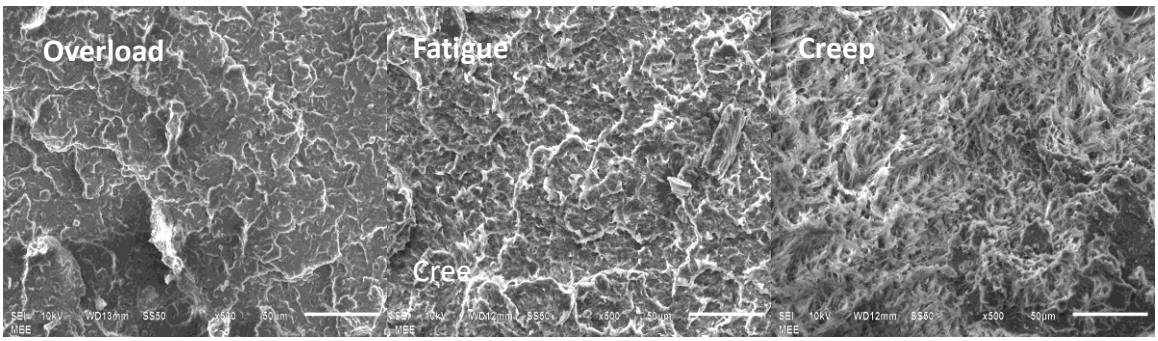

Figure 47: Micrographs from the overload, fatigue, and creep samples. All of these images are from the lower quarter of the fracture surface where .25w > a.

Evaluating the area of the fracture surface near the midpoint shows some changes in the characteristics of the different samples. Images from this region of each of the three samples are shown in Figure 48. At this point in crack advance the overload and fatigue samples diverge in character. The fatigue sample is starting to show alignment of the surface striations as the crack begins to advance from the inner edge of the clip slot rather than the bottom of the sample. Clear orientation is evident at this point in the sample. In contrast, while the overload sample shows definite linear edges, they do not show consistent alignment. The creep sample, in contrast, at this point looks very similar to the overloaded sample at this scale. This is likely due to the fact that at the

load applied to the creep sample, fast fracture initiated as a relatively short crack length and by this point in the sample the creep portion of the failure was already complete. In order to distinguish between the creep and overloading failure modes it would be important to look at the entire fracture surface to note the surface morphology shown in Figure 47 rather than the relatively similar surfaces after the creep phase of crack progression.

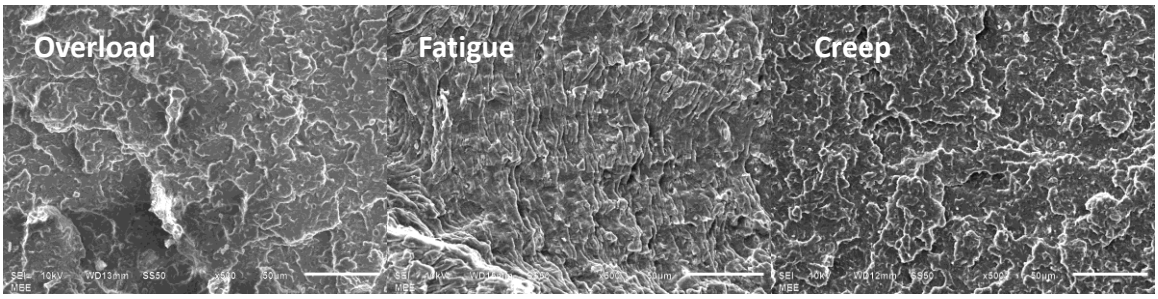

Figure 48: Micrographs from the overload, fatigue, and creep samples. All of these images are from the middle of the fracture surface where .25 w > a > .5 w

Near the termination point of the crack, again we see a divergence in surface morphology. As the crack length approaches w and the stress intensity rises, the fatigue sample shows a transition in crack progression from fatigue striations to overload failure. The overload sample shows multiple arcs of different z heights radiating from the inner wall of the clip groove, indicating a very dynamic crack growth regime while the creep sample looks relatively the same as it did at smaller *a* lengths. This indicates that the overloading condition itself (as experienced by all three samples during final crack propagation) can yield different surface morphologies. This may indicate that different mechanisms of local deformation are operating in each case- perhaps

spherulitic fracture in the case of the smoother surfaces and fracture of the amorphous regions surrounding the spherulites in the more rough overload surface. Crack advance around the spherulites may help to explain the greater level of variation in crack surface height in that sample.

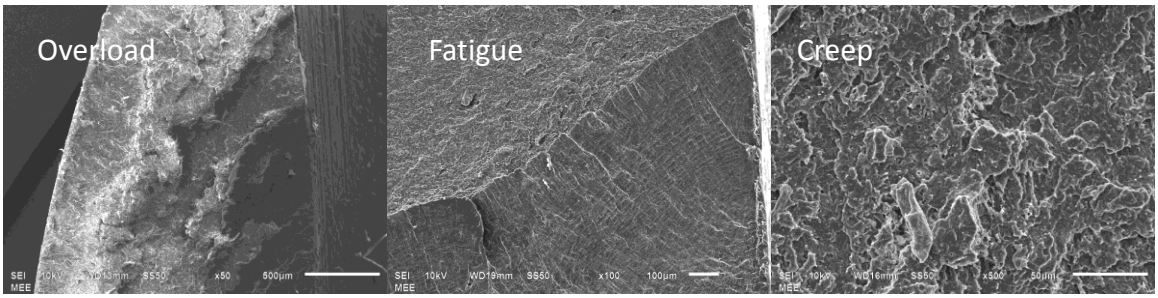

Figure 49: Micrographs from the overload, fatigue, and creep samples. All of these images are from the stage of crack growth where a > .5 w.

Summary of Surface Morphology:

The analysis of real product samples that were intentionally fractured using known, controlled methods has revealed surface features that appear to be characteristic of the failure modes applied. This will allow more accurate determination of the cause of failure of samples which have fractured in the field, where the mechanism of failure is unknown.

The presence of striations emanating from the interior edge of the clip groove and changing orientation by roughly 90 degrees as the crack progresses can be taken as evidence of fatigue loading. However, the appearance of striations over small portions of the sample could be confused with the normal morphology of an overloading fracture, so longer distances and multiple areas of the sample would need to be analyzed in order to accurately identify whether fatigue is presence.

The presence of a section of the surface with the fibrils shown in Figure 42 and Figure 47 is strong evidence of a creep failure, while the presence of crazes as shown in Figure 41 would provide additional confirmation.

A part which displays a relatively featureless fracture surface like that of Figure 46, perhaps with a smooth, glassy initiation point would likely have failed through simple overloading.

Accurately determining the failure mechanism gives valuable insight into the likely installation conditions that would have been associated with or even responsible for the fracture of a returned sample. This information would be of great benefit in a judicial proceeding where fault is apportioned.

Conclusions

While it is clear from the difficulty of attempts to generate failures that the acetal material used in this product is robust, it is also clear from the number of returns that fractures are nevertheless possible. From a design perspective, however, it appears that acetal provides unique advantages in terms of its high crystallinity, providing resistance to solvents and chemical attack, its resistance to fatigue, and its resistance to creep. Indeed, it was very difficult to generate failures based upon fatigue and creep loading without either not causing the sample to fracture or all, or instead causing it to fracture via a different mechanism (overloading).

Under appropriate conditions both creep and fatigue mechanisms can operate in such a way as to cause the initiation of a crack, and that once that crack is formed those same mechanisms can drive it to propagate until failure. During crack propagation, any stress condition present will serve to assist in the advance of the crack. Whether the crack progresses quickly or slowly depends only upon the magnitude of those stresses.

By finding a successful test condition to generate both fatigue and creep failures in actual parts rather than test plaques or dogbone samples, it is now possible to compare field fractured parts with unknown failure modes to known samples and more accurately discern the mechanism of fracture without the need to extrapolate from different part shapes or wall thicknesses. This evidential base will provide a useful

touchstone in failure analysis of parts from the field. It will also be more persuasive in judicial matters in that it is based upon actual experimental evidence rather than opinion, estimation, or experience with other parts with varying degrees of similarity.

Future work to be considered could include defining the number of fatigue cycles necessary to nucleate a crack using different load cycles at different stress intensity factors, and at different temperatures to determine conditions most favorable to crack initiation. Additional creep testing could be done with different loads over different time periods to better simulate long service lives to determine when cracks begin to nucleate and grow stably. A refined FEA analysis using detailed plastic or viscoelastic material models to identify accurate stress levels at realistic loading conditions, and correlating the fatigue crack initiation data and FEA simulations to published or experimental threshold ΔK values.

Bibliography

Alessandro Pegoretti, T. R. (1999). Fatigue Crack Propagation in Polypropylene Reinforced with Short Glass Fibers. *Composite Science and Technology , 59*, 1055-1062.

C. F. Hammer, T. A. (1959). Fine Structure of Acetal Resins and Its Effect on Mechanical Properties. *Journal of Applied Polymer Science , 1* (2), 169-178.

Chemfinder. (2008, September 23rd). Retrieved September 23rd, 2008, from Chemfinder.com: http://chembiofinderbeta.cambridgesoft.com/Search.aspx?SearchCriteriaId=5&SearchCriteriaValue=formaldehyde

Christopher J.G. Plummer, P. S.-H. (2000). High Temperature Slow Crack Growth in Polyoxymethylene. *Polymer Engineering and Science , 40* (6), 1306-1317.

Dupont Engineering Polymers. (2006, November). *Dupont Delrin Technical Literature.* Retrieved February 10, 2009, from Dupont Corporation Web Site.

Gohil, R., Patel, K., & Patel, R. (1974). Plastic Deformation of Polyoxymethylene Crystals. *Colloid and Polymer Science , 252*, 358-366.

Goodman, W. L. (1959). Physical Properties of High Molecular Weight Acetal Resins. *Journal of Applied Polymer Science , 1* (2), 179-184.

Hertzberg, R. W. (1996). *Deformation and Fracture Mechanics of Engineering Materials.* New York: John Wiley and Sons.

Jones, N., & Lesser, A. (1998). Morphological Study of Fatigue-Induced Damage in Isotactic Polypropylene. *Journal of Polymer Science, Part B: Polymer Physics , 36*, 2751-2760.

K. Mao, C. J. (2006). Acetal gear wear and performance prediction under unlubricated running condition. *Jounal of Synthetic Lubrication* (23), 137-152.

Katti, S., & Schultz, J. (1982). The Microstructure of Injection Molded Semicrystalline Polymers: A Review. *Polymer Engineering and Science* , 1001-1016.

M.N. Riddell, G. K. (1966, October). Fatigue Mechanisms of Thermoplastics. *Polymer Engineering and Science* , 363-368.

Patel, N. A. (1993). *Subcritical Phase Characterization of Delrin Acetal Resin.* Long Beach, CA: California State University.

Price, S. B. (1970). *Polyacetals.* London: Iliffe Books.

R. G. Alsup, J. P. (1959). The Effect of Solvents on High Molecular Weight, Stable Acetal Resins. *Journal of Applied Polymer Science , 1* (2), 185-191.

Roel P. M. Janssen, D. d. (2008). Fatigue Life Prediction for Glassy Polymers: A Constituitive Approach. *Macromolecules , 41* (7), 2520-2530.

Russel B. Akin. (1962). *Associate Director, Technical Services Library at E.I. duPont de Nemours.* New York: Reinhold Publishing Corporation.

S. J. Barker, M. P. (1970). *Polyacetals.* London: Iliffe Books.

S.S. Kati, J. S. (1982). The Microstructure of Injection Molded Semicrystalline Polymers: A Review. *Polymer Engineering and Science , 22* (16), 1001-1017.

Schultz, J. (1984). Microstructural Aspects of Failure in Semicrystalline polymers. *Polymer Engineering and Science , 24* (10), 770-785.

Schultz, J. (1984). Microstructural Aspects of Failure in Semicrystalline Polymers. *Polymer Engineering and Science* , 770-785.

The Lee Company. (2009). *IMH Handbook of Hydraulics and Pneumatics 3rd Edition.* Westbrook, CT.
Ticona/Celanese Corporation. (2009, November 10). *Ticona Product Tool*. Retrieved November 10, 2009, from www.tools.ticona.com/tools/mcbasei/product-tools.php
Zhurkov S.N., K. V. (1969). Formation of Submicrocracks in Polymers Under Load. *Soviet Physics- Solid State , 11* (2), 296-307.

Appendix A:

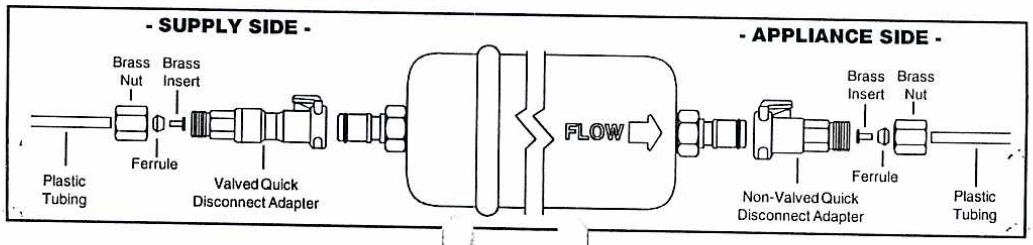

TOOLS REQUIRED FOR INSTALLATION

(2) Adjustable Wrenches
Pipe Cutter
File or Sandpaper

1. Shut off water supply.
2. Select location for installation. Supply line normally will be a 1/4 inch O.D. (outside diameter) plastic or soft copper line which is connected to your household water line. The filter will require a minimum of three (3) inches behind the appliance.
3. Cut incoming 1/4 inch O.D. tubing where you want to install the filter. Deburr cut ends with file or sand paper.
4. If copper tubing, remove nuts and ferrules (small plastic sleeves) from package. Slide brass nuts onto ends of soft copper tubing then slide plastic ferrules onto tubing (short taper toward brass nut). If water line is 1/4 inch O.D. plastic tubing instead of soft copper tubing, place the brass nut and plastic ferrule on the tubing and then insert the enclosed brass insert into the end of the plastic tubing.
5. Insert end of the supply-side tubing into the threaded side of the valved quick-disconnect adapter as far as it will go. Slide ferrule and nut down to threads and hand tighten nut onto compression fitting. Tubing must be pushed all the way into fitting while tightening nut. Use two wrenches to final tighten the compression nut at least one full turn.
6. Repeat steps 4 and 5 for the appliance side non-valved quick-disconnect adapter.
7. See IC-101 packaging for installation instructions.

Figure 50: Installation instructions for Ametek IC-101 water filter.

GE SmartWater™

INSTALLATION INSTRUCTIONS

GE Model GXRTQ and GXRTQR Filters

Your new GE icemaker water filter comes complete with all the necessary hardware for installation.
Each filter gives you up to six months of great-tasting water. Filter should be changed after 6 months of use.

REQUIRED TOOLS FOR INSTALLATION

- a tube cutter
- 7/16" and 1/2" wrenches
- a knife
- a bucket or pan

OPTIONAL TOOLS FOR INSTALLATION

- a file
- sandpaper

CAUTION: Using pliers or vise grips WILL damage the fittings.

WARNING

Do not use where water is microbiologically unsafe or with water of unknown quality without adequate disinfection before or after the filter.

Small parts remaining after the installation could be a choke hazard. Discard safely.

NSF

System tested and certified by NSF international against ANSI/NSF Std. 42 for the reduction of chlorine and taste and odor.

SPECIFICATIONS

- This System has been tested according to ANSI/NSF 42 for reduction of the substances listed below. The concentration of the indicated substances in water entering the system was reduced to a concentration less than or equal to the permissible limit for water leaving the system, as specified in ANSI/NSF 42.
- Actual performance may vary with local water conditions.

Model	Service Flow rate	Service Life	Pressure	Max. Temp.	Contaminant	Tested % Reduction	% Reduction Required	Influent Challenge Concn. Required	Average Influent	Average Effluent
GXRTQ GXRTQR	0.5 gpm (1.9 lpm)	2000 gal. (7571 liters) or 6 months	25–125 psi (172–862 kPa)	100°F. (38°C.)	Chlorine	99%	≥75%	2.0 mg/L ± 10%	2.0 mg/L	0.1 mg/L

Testing parameters: Influent Challenges = pH 7.5 ± 0.5; Temperature 68°F ± 5°F (20°C ± 3°C); Pressure 60 psig; Flow Rate = 1 gpm
If slow water or hollow ice occurs, replace filter.

INSTALLATION PRECAUTIONS

- Protect from freezing. Drain filter when room temperature drops below 32°F. (0°C.).
- Use the in-line water filtering system on a potable, safe-to-drink, home COLD water supply only. The filter will not make unsafe water safe to drink. Do NOT use on HOT water (100°F. max.).
- Do not install on line pressure above 125 psi (862 kPa), or below 25 psi (172 kPa).
- All of the refrigerator installation requirements must be met when installing the filter.
- Do not install in direct sunlight.
- Installation must comply with existing state or local plumbing codes.
- It is essential that operational, maintenance and filter replacement requirements be carried out for this product to perform as advertised. Change filter at least every six months. Flush new cartridge for 5 minutes.

LIMITED 60 DAY WARRANTY

- *What does this warranty cover?*
  - — Any defect in materials or workmanship in the manufactured product.
- *What does this warranty not cover?*
  - — Filter Cartridges.
  - — Service trips to your home to teach you how to use the product.
  - — Improper installation.
  - — Failure of the product if it is abused, misused, altered or used for other than the intended purpose.
  - — Defects that result from improper installation or damage not caused by GE.
  - — Liability on the part of GE under this or any other warranty for any indirect or consequential damage.
  - — Products that are used for commercial or industrial applications.
  - — Use of this product where water is microbiologically unsafe or of unknown quality, without adequate disinfection before or after the system. Systems certified for cyst reduction may be used on disinfected water that may contain filterable cysts.
  - — Damage to the product caused by accident, fire, floods or acts of God.
  - — Incidental or consequential damage caused by possible defects with this appliance, its installation or repair.
- *For how long after the original purchase?*
  - — Sixty (60) days.
- *How do I make a warranty claim?*
  - — Return to the retailer from which it was purchased, along with a copy of the "Proof of Purchase." This warranty excludes the cost of shipping or service calls to your home.
- *How does state law relate to this warranty?*
  - — This warranty gives you specific legal rights, and you may also have other rights which vary from state to state. THIS WARRANTY IS INTENDED TO BE IN LIEU OF ALL OTHER WARRANTIES, WHETHER EXPRESS OR IMPLIED, INCLUDING THE WARRANTIES OF MERCHANTABILITY AND FITNESS FOR A PARTICULAR PURPOSE.

Contact us at ge.com, or call 800.GE.CARES (800.432.2737) in the U.S., or toll-free 866.777.7627 in Canada.

147099 251B6017P005 (08-05 JR) 49-50073-2

ge.com

GENERAL ELECTRIC COMPANY, Appliance Park, Louisville, KY 40225

Figure 51: Installation instructions for GE GXRTQ water filter, page 1.

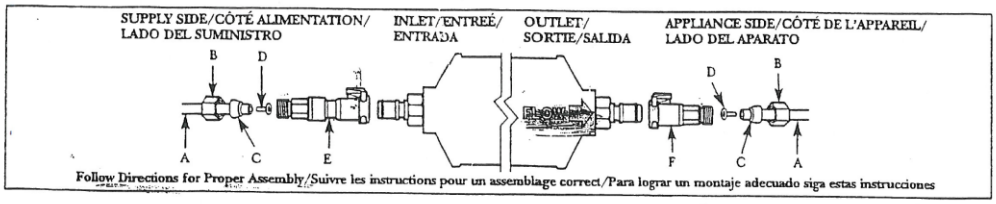

Follow Directions for Proper Assembly/Suivre les instructions pour un assemblage correct/Para lograr un montaje adecuado siga estas instrucciones

INSTALLING THE FILTER

1. All of the refrigerator installation requirements must be met when installing the filter.

Cut Tubing

2. Shut off water supply.
3. The filter is to be inserted (spliced) into the 1/4" OD supply tube that feeds water to the refrigerator. (Do not cut any water lines internal to the refrigerator.) Locate the filter as close as possible to the supply water shut-off valve. If the filter needs to be located behind the refrigerator, there needs to be at least 6 inches of clearance between the wall and the refrigerator. If the appliance must be moved, make sure there is proper protection on the floor.
4. Cut the tubing (A), making sure the ends are square and no burrs protrude. Deburr ends with file or sandpaper if necessary.

Attach Fittings to Tubing

5. Slip brass nuts (B) then ferrules (C) over both tubing (A) ends, leaving 1/4" of tubing exposed from end. (See figure for ferrule orientation). If your tubing is plastic, place brass inserts (D) into ends of tubing.
6. *a.* Insert end of supply side tubing into the valved fitting (E) (the ***longer*** fitting); hand-tighten nut onto threads of fitting.

   CAUTION: Be careful not to cross thread the nut and the fitting.

   b. Using two wrenches, tighten nut at least one full turn.

   c. Valved fitting (E) is now installed. Turn water supply on and inspect for leaks.

   d. Repeat *a* and *b* for non-valved fitting (F) on the appliance side.

Flush Filter

7. Place filter outlet over bucket or pan; fine particles of carbon may be present—***flush*** by connecting filter ***inlet*** to valved fitting. Fine carbon particles will be removed during the flushing. Disconnect inlet to stop flushing after 2 to 3 gallons of water are flushed (approx. 5 minutes).

Final Connection and Leak Check

8. Connect the ***outlet*** of the filter to the water line going to your refrigerator.
9. Connect the inlet of the filter to the water supply line and inspect for leaks. If a leak occurs, tighten nuts or fittings until the leak stops.
10. Write the date on the filter and also mark your calendar to replace with another filter after six months.

PROCEDURE FOR REPLACING THE FILTER

1. Get a bucket and a towel.
2. Disconnect the old filter at its ***inlet*** first and then its outlet. Water source will shut off automatically, but some water may spill or drip back through the filter.
3. Place filter outlet over bucket; fine particles of carbon may be present—***flush*** by connecting filter ***inlet*** to valved fitting. Fine carbon particles will be removed during the flushing. Disconnect inlet to stop flushing after 2 to 3 gallons of water are flushed (approx. 5 minutes).
4. Connect the filter ***outlet*** first, then reconnect the inlet.

   Write the date on the filter and also mark your calendar to replace with another filter after six months.

INSTALLATION DU FILTRE

1. Lors de l'installation du filtre, on doit respecter toutes les exigences concernant l'installation du réfrigérateur.

Coupe du tube

2. Fermer l'arrivée d'eau.
3. Raccorder le filtre au tube d'arrivée d'eau au réfrigérateur (dia. ext. 1/4 po). (Ne sectionner aucune canalisation d'eau interne du réfrigérateur.) Placer le filtre aussi près que possible du robinet d'arrêt de la canalisation d'eau. S'il est nécessaire de placer le filtre derrière le réfrigérateur, prévoir un espace libre d'au moins 6 po entre le réfrigérateur et le mur. S'il est nécessaire de déplacer l'appareil, veiller à bien protéger le plancher.
4. Couper le tube (A) – Veiller à l'équerrage et à l'absence de bavures. Si nécessaire, éliminer les bavures avec une lime ou du papier abrasif.

Connexion des tubes sur les raccords

5. Sur chaque extrémité de tube (A), enfiler l'écrou (B) et la virole (C) de laiton; laisser le tube dépasser de 1/4 po (pour l'orientation de la virole, voir l'illustration). Pour les tubes de plastique, insérer un petit tube de laiton (D) dans l'extrémité.
6. *a.* Insérer l'extrémité du tube (côté alimentation) dans l'ensemble raccord/robinet (E) (le raccord le ***plus long***); serrer l'écrou à la main sur le filetage.

   MISE EN GARDE : Veiller à ne pas détériorer le filetage, l'écrou ou le raccord.

   b. Utiliser deux clés pour serrer l'écrou d'au moins un tour complet.

   c. L'ensemble raccord/robinet (E) est maintenant installé. Ouvrir l'arrivée d'eau; inspecter pour rechercher les fuites.

   d. Répéter les étapes *a* et *b* pour le raccord sans robinet (F), du côté de l'appareil.

Rinçage du filtre

7. Placer l'ouverture de sortie du filtre au-dessus d'un seau ou récipient; de fines particules de carbone peuvent être présentes—***pour rincer***, connecter ***l'entrée*** du filtre au raccord/robinet. De fines particules de carbone seront entraînées durant ce rinçage. Effectuer le rinçage pendant environ 5 minutes (2 à 3 gallons d'eau), puis déconnecter.

Raccordement final et recherche des fuites

8. Connecter la ***sortie*** du filtre à la canalisation d'eau qui alimente le réfrigérateur.
9. Connecter l'entrée du filtre à la canalisation d'arrivée d'eau; inspecter pour rechercher les fuites. S'il y a des fuites, resserrer les écrous ou raccords pour éliminer chaque fuite.
10. Inscrire la date d'installation sur le filtre; noter également sur un calendrier la date à laquelle il faudra remplacer le filtre–dans six mois.

REMPLACEMENT DU FILTRE

1. Disposer d'un seau et d'une serviette.
2. Déconnecter le vieux filtre – à l'entrée d'abord, puis à la sortie. L'arrivée d'eau sera automatiquement interrompue, mais un peu d'eau peut se renverser ou sortir du filtre.
3. Placer l'ouverture de sortie du filtre au-dessus d'un seau; de fines particules de carbone peuvent être présentes—***pour rincer***, connecter ***l'entrée*** du filtre au raccord/robinet. De fines particules de carbone seront entraînées durant ce rinçage. Effectuer le rinçage pendant environ 5 minutes (2 à 3 gallons d'eau), puis déconnecter.
4. Connecter d'abord la ***sortie*** du filtre, puis l'entrée.
5. Inscrire la date d'installation sur le filtre; noter également sur un calendrier la date à laquelle il faudra remplacer le filtre–dans six mois.

CÓMO INSTALAR EL FILTRO

1. Es necesario cumplir con todos los requisitos de instalación del refrigerador al instalar el filtro.

Cómo cortar la tubería

2. Cierre el suministro de agua.
3. El filtro debe colocarse (empalmarse) en la línea de suministro de agua de 1/4" OD (diámetro externo) hacia el refrigerador. (No corte ninguna línea de agua en el interior del refrigerador.) Ubique el filtro los más cerca posible de la válvula de cierre del agua. Si el filtro debe instalarse detrás del refrigerador, deberá haber un espacio libre mínimo de 6 pulgadas (15 cm) entre la pared y el refrigerador. Cerciórese de que dispone de una protección del piso adecuada si necesita mover el aparato electrodoméstico.
4. Corte la tubería (A) y cerciórese que los extremos están planos y que no sobresale ninguna rebaba. Si es necesario, desbarbe bien los extremos con una lima o papel de lija.

Cómo pegar los acopladores a las tuberías

5. Deslice las tuercas de latón (B) y luego los casquillos anulares (C) sobre ambos extremos de la tubería (A), dejando 1/4" de tubería expuesta en cada extremo. (Vea la figura para la orientación de la férula). Coloque las inserciones de latón (D) en los extremos de la tubería, si ésta es de plástico.
6. *a.* Inserte el extremo de la tubería del lado del suministro en el acoplador con válvula (E) (el acoplador ***más largo***); apriete a mano la tuerca en la rosca del acoplador.

   PRECAUCION: Tenga cuidado de no cruzar el hilo de la tuerca con el del acoplador.

   b. Apriete la tuerca cuando menos una vuelta completa utilizando dos llaves de tuercas.

   c. Con esto quedó instalado el acoplador de válvula (E). Abra el suministro de agua y compruebe que no haya fugas.

   d. Repita el proceso de *a* y *b* para el acoplador sin válvula (F) del lado del aparato electrodoméstico.

Enjuague el filtro

7. Coloque la salida del filtro en una cubeta o bandeja cacerola; pequeñas partículas de carbón pudieran estar presentes—***enjuague*** conectando la ***entrada*** del filtro al acoplador con válvula. Las pequeñas partículas de carbón se eliminarán durante este proceso. Desconecte la entrada para parar el paso del agua después de usar 2 o 3 galones (aprox. 5 minutos).

Conexión final y revisión de goteras

8. Conecte la ***salida*** del filtro a la tubería que conduce el agua hacia su refrigerador.
9. Conecte la entrada del filtro a la línea de suministro de agua y compruebe que no haya fugas. Si se presentara alguna fuga, apriete las tuercas o los acopladores hasta que cesen las fugas.
10. Escriba la fecha en el filtro y también anótela en su calendario para recordar que debe reemplazar el filtro después de seis meses.

PROCEDIMIENTO PARA REEMPLAZAR EL FILTRO

1. Consiga una cubeta y una toalla.
2. Desconecte el filtro viejo, empezando por el extremo de ***entrada*** y después el de salida. La fuente de suministro de agua se cerrará automáticamente, aunque algo de agua pudiera regarse o gotear a través del filtro.
3. Coloque la salida del filtro en una cubeta; pequeñas partículas de carbón pudieran estar presentes—***enjuague*** conectando la ***entrada*** del filtro al acoplador con válvula. Las pequeñas partículas de carbón se eliminarán durante este proceso. Desconecte la entrada para parar el paso del agua después de usar 2 o 3 galones (aprox. 5 minutos).
4. Conecte primero el lado de la ***salida*** del filtro y después reconecte la entrada.
5. Escriba la fecha en el filtro y también anótela en su calendario para recordar que debe reemplazar el filtro después de seis meses.

Figure 52: Installation instructions for GE GXRTQ water filter, page 2.